CR-152094

Department of Aerospace Engineering

University of Cincinnati

(NASA-CR-152094) OPTIMIZATION STUDY FOR HIGH SPEED RADIAL TURBINE WITH SPECIAL REFERENCE TO DESIGN VARIABLES (Cincinnati Univ.) 67 p HC A04/MF A01 CSCL 21E N78-17063

Unclas G3/07 04789

OPTIMIZATION STUDY FOR HIGH SPEED RADIAL TURBINE WITH SPECIAL REFERENCE TO DESIGN VARIABLES

BY

I. KHALIL AND W. TABAKOFF

Supported by:

NATIONAL AERONAUTICS AND SPACE ADMINISTRATION

Ames Research Center

U.S. Army Air Mobility Research & Development Laboratory

Moffett Field, California

Contract No. NAS2-7850

OPTIMIZATION STUDY FOR HIGH SPEED RADIAL TURBINE WITH SPECIAL REFERENCE TO DESIGN VARIABLES

by

I. Khalil and W. Tabakoff

Supported by:

NATIONAL AERONAUTICS AND SPACE ADMINISTRATION

Ames Research Center

U.S. Army Air Mobility Research & Development Laboratory

Moffett Field, California

Contract No. NAS2-7850

1. Report No.	2. Government Accession No.	3. Recipient's Catalog No.
4. Title and Subtitle OPTIMIZATION STUDY FOR HIGH SPEED RADIAL TURBINE WITH SPECIAL REFERENCE TO DESIGN VARIABLES		5. Report Date October 1977 6. Performing Organization Code
7. Author(s) I. Khalil and W. Tabakoff		8. Performing Organization Report No.
9. Performing Organization Name and Address Department of Aerospace Engineering & Applied Mechanics University of Cincinnati Cincinnati, Ohio 45221		10. Work Unit No. 11. Contract or Grant No. NAS2-7850
12. Sponsoring Agency Name and Address National Aeronautics & Space Administration Washington, D.C. 20546 and U.S. Army Air Mobility Research & Development Laboratory Moffett Field, California 94035		13. Type of Report and Period Covered 14. Sponsoring Agency Code

15. Supplementary Notes

16. Abstract

Numerical results of a theoretical investigation are presented to provide information about the effect of variation of the different design and operating parameters on radial inflow turbine performance. The effects of variations in the mass flow rate, rotor tip Mach number, inlet flow angles, number of rotor blades and hub to shroud radius ratio, on the internal fluid dynamics of turbine rotors, was investigated. A procedure to estimate the flow deviation angles at the turbine exit is also presented and used to examine the influence of the operating conditions and the rotor geometrical configuration on these deviations. The significance of the results obtained are discussed with respect to improved turbine performance.

17. Key Words (Suggested by Author(s))	18. Distribution Statement
Radial Turbine Internal Fluid Dynamics in Radial Turbines	Unclassified - unlimited

19. Security Classif. (of this report)	20. Security Classif. (of this page)	21. No. of Pages	22. Price*
Unclassified	Unclassified	62	

* For sale by the National Technical Information Service, Springfield, Virginia 22161

NASA-C-168 (Rev. 10-75)

ORIGINAL PAGE IS
OF POOR QUALITY

TABLE OF CONTENTS

	Page
SUMMARY	1
INTRODUCTION	2
PART I: FLOW ANALYSIS WITHIN BLADE PASSAGES	
GENERAL	3
MERIDIONAL FLOW SOLUTION	4
BLADE TO BLADE SOLUTION	5
CONDITIONS OF SOLUTION	6
PRESENTATION OF RESULTS AND DISCUSSION	7
MERIDIONAL RESULTS	7
BLADE SURFACE VELOCITY DISTRIBUTION	9
EFFECT OF CHANGING NUMBER OF BLADES	9
EFFECT OF MASS FLOW RATE	10
EFFECT OF VARIABLE ROTOR TIP MACH NUMBER	11
EFFECT OF VARIABLE STATOR ANGLE ON TURBINE PERFORMANCE	12
PART II. ANALYTICAL STUDY OF THE FLOW DISTRIBUTION AT EXIT FROM THE TURBINE ROTOR	
PRELIMINARY CONSIDERATIONS	13
ANALYSIS	14
GOVERNING EQUATIONS	14
ASSUMPTIONS AND LIMITATIONS FOR THE ANALYTICAL SOLUTION	16
ESTIMATION OF THE RELATIVE SWIRL VELOCITY DISTRIBUTION	20
RESULTS AND DISCUSSION	22
PASSAGE AVERAGED VALUE OF SWIRL VELOCITY AT ROTOR EXIT	22
FLOW ANGLE DISTRIBUTION AT ROTOR EXIT	24

REFERENCES 26

LIST OF SYMBOLS 27

TABLES 29

FIGURES 32

SUMMARY

Numerical results of a theoretical investigation are presented to provide information about the effect of variation of the different design and operating parameters on radial inflow turbine performance. The effects of variations in the mass flow rate, rotor tip Mach number, inlet flow angles, number of rotor blades and hub to shroud radius ratio, on the internal fluid dynamics of turbine rotors, was investigated. A procedure to estimate the flow deviation angles at the turbine exit is also presented and used to examine the influence of the operating conditions and the rotor geometrical configuration on these deviations. The significance of the results obtained are discussed with respect to improved turbine performance.

INTRODUCTION

The benefits of using small radial inflow turbines in conjunction with automotive and aeronautical industries have been discussed by many authors [1, 2]. Boundary layer separation, secondary flow effects and heat transfer problems within the flow channels of these machines are examples of factors which impose a limit on their efficiency. These factors could be controlled by aerodynamic design methods based upon detailed knowledge of the flow behavior within the different passages of the turbine. Both theoretical and experimental investigations of flow conditions that result from various design configurations and operating parameters are considered necessary to develop this knowledge.

In the present work a theoretical study, which makes use of recent advances in computational fluid mechanics, is presented. The object is to improve our understanding of the internal fluid dynamics of radial inflow turbine rotors under different operating conditions. A single stage rotor having a pressure ratio of 3.0 to 1 is used as a model in this study. The effects of variations in the following design and operating parameters upon the rotor performance are investigated:

a. Turbine flow rate
b. Rotor tip Mach number
c. Number of rotor blades
d. Inlet flow angles to the rotor
e. Hub to shroud radius ratio.

The flow field analysis procedure and the computer program employed, to test the effect of the different parameters, are identical to that presented in Ref. [3]. Basically, the procedure is based upon the solution of the velocity gradient equation along an arbitrary quasi-orthogonal in the meridional plane. From this meridional flow solution the blade surface velocities are obtained according to the method presented in Ref. [4]. The factors which govern the selection of this procedure have been discussed in Ref. [5]. The assumptions made in Ref. [3] yield to a solution of the flow

field which give good results only for the velocity distribution within the blade channels, away from turbine exit.

Due to the peculiarity of the method of analysis of Ref. [3] in detecting the real flow behavior at turbine exit, an analytical model is developed in Part 2 of this study. The model offers a procedure whereby the flow deviation from blade surface at turbine exit is estimated. The model is based on the analytical solution of the governing equations of two dimensional irrotational motion of flow between blades with some simplifying assumptions. The solution obtained allows also for the calculation of flow parameters at turbine exit in a quantitative manner, with a more realistic dependence on the geometrical configuration and operating conditions. It is hoped that the results of the parametric study presented in Part 1, together with the application of the proposed model, yield an improved design procedure for the radial turbine.

PART I - FLOW ANALYSIS WITHIN BLADE PASSAGES

General

The detailed knowledge of the flow behavior through turbomachines can be achieved through a field analysis of the unsteady, rotational, three dimensional viscous flow. One approach would be to attempt the solution of the complete Navier Stokes equations. Clearly, such solution is out of reach now and in the immediate future. An alternative approach which has been widely used is to assume that a two layer model is representative, i.e. an inviscid flow solution which interacts with an end wall boundary layer solution.

Three dimensional inviscid flow analyses usually involve a combination of several two-dimensional solutions on intersecting families of stream surfaces [5]. Most two-dimensional solutions are either on a blade-to-blade surface of revolution or on the mid-channel stream surface between two blades (Fig. 1).

In the following study, the internal fluid dynamics of turbine rotors are investigated under different operating conditions. The viscous effects are neglected. The solution to

the equations of inviscid flow on the mid-channel surface is obtained using the quasi-orthogonal method [3]. This solution is termed here the "meridional flow solution". Using this solution, the blade surface velocities are obtained.

Meridional Flow Solution

The flow field analysis procedure presented in Ref. [3], and employed here to study the flow behavior in the meridional plane of turbine rotors, is based on the streamline curvature method. In this method, the velocity gradient equation along a quasi-orthogonal is integrated numerically to calculate the distribution of flow properties. The governing equation for the velocity gradient is given as follows:

$$\frac{dW}{ds} = \left(A \frac{dr}{ds} + B \frac{dz}{ds}\right) W + C \frac{dr}{ds} + D \frac{dz}{ds} + \left(\frac{dh_2}{ds} - \omega \frac{dY}{ds}\right) \frac{1}{W} \qquad (1)$$

where

$$A = \frac{\cos\alpha \cos^2\beta}{r_c} - \frac{\sin^2\beta}{r} + \sin\alpha \sin\beta \cos\beta \frac{\partial\theta}{\partial r}$$

$$B = - \frac{\sin\alpha \cos^2\beta}{r_c} + \sin\alpha \sin\beta \cos\beta \frac{\partial\theta}{\partial z}$$

$$C = \sin\alpha \cos\beta \frac{dW_m}{dm} - 2\omega \sin\beta + r\cos\beta \left(\frac{dW_\theta}{dm} + 2\omega \sin\alpha\right) \frac{\partial\theta}{\partial r}$$

$$D = \cos\alpha \cos\beta \frac{dW_m}{dm} + r\cos\beta \left(\frac{dW_\theta}{dm} + 2\omega \sin\alpha\right) \frac{\partial\theta}{\partial z} \qquad (2)$$

The coordinate system and the notations are shown in Figure 2.

The numerical solution to equation (1) is assumed to be valid for the mean stream surface which extends from hub to shroud. This mean flow surface is considered to be parallel to the mean blade surface. Empirical corrections are made to take into account the difference between the actual flow angle and the blade angle at inlet to the rotor. No provisions have been reported in Ref. [3] to take care of this difference at the turbine exit. In view of this fact, it is felt that it is quite meaningful to study the mechanism which causes the

flow deviation from blade surface, at turbine exit, on a rigorous basis. In the second part of the present study, a calculation procedure will be developed to predict these flow deviations so that appropriate measures may be taken to improve the flow calculations.

Blade to Blade Solution

In order to render a rational judgement with regard to the effect of variation of the different design parameters upon the performance of the turbine rotor, knowledge of the velocity distribution over the rotor blades is necessary. With the velocities on the mean stream surface calculated according to equations (1) and (2), the blade surface velocities can be obtained by several methods. One that gives good results, when compared with the relaxation solution of the potential flow equation, is given by Stantiz [4]. His method is based on absolute irrotational flow and linear velocity distribution between blades. The following equations based on these assumptions are used, herein, to obtain the required blade surface velocities.

$$W_s = \frac{\cos\beta_s \cos\beta_p}{\cos\beta_s + \cos\beta_p} \left\{ \frac{2W}{\cos\beta_p} + \omega r(\tan\beta_s - \tan\beta_p) + \frac{d}{dm}\left[(\omega r + W\sin\beta)\left(\frac{2\pi r}{Z} - t_\theta\right)\right] \right. \tag{3}$$

and

$$W_p = 2W - W_s \tag{4}$$

In these equations, the velocity W and the flow angle β are those obtained from the meridional flow solution. The subscripts "s" and "p" refer to the suction and the pressure surfaces, respectively.

Conditions of the Solution

The flow behavior within the channels of a radial inflow turbine rotor is investigated under different operating conditions. The solutions which will be presented are intended to show the effects upon the rotor performance of variations in the following parameters:

1. Turbine flow rate
2. Rotor tip Mach number
3. Number of rotor blades
4. Inlet flow angles to the rotor.

The rotor considered in this study has a hub-shroud profile in the meridional plane similar to that shown in Figure 3a. Table 1 summarizes the ranges over which the different parameters are varied. The standard solution presented in the Table corresponds to the following estimated operating conditions (design point of the turbine):

Turbine inlet total pressure, P_{t2}	=	42.5 lb/in^2
Turbine inlet total temperature, T_{t2}	=	2710°R
Turbine pressure ratio	=	3.0
Rotational speed, r.p.m.	=	79,800 r.p.m.
Turbine mass flow rate, Q	=	0.932 lb/sec
Stator nozzle exit flow angle, α_2 (inlet to the rotor)	=	73.0 degrees
Working fluid	=	Air

Other design point conditions needed for the analysis were determined theoretically from the previous data, and are given as follows:

The angle between relative velocity vector and its meridional component at rotor inlet, β_2	=	-40.91 degrees
Absolute fluid velocity at rotor inlet, V_2	=	1575 ft/sec
Equivalent weight flow, $(\dot{Q}\sqrt{\theta}/\delta)$	=	0.735 lb/sec
Prewhirl at the rotor inlet, $V_{\theta_2} \cdot r_2$	=	346.98 ft^2/sec
Additional drop in total pressure across the turbine rotor due to losses	=	2.5 lb/in^2

In order to obtain the reference conditions for the different operating cases of Table 1, a computer program is developed. The program requires as an input the stator and rotor geometries, the mass flow rate, the rotational speed, and the total conditions to the turbine. It calculates, through an iterative procedure using a one dimensional analysis, the absolute fluid velocity, V_2, the angle β_2, and the prewhirl at the rotor inlet, $V_{\theta_2} r_2$. These values are used as input data for the computer program of Ref. [3]. A sample input to the program, for the turbine under consideration at the design point, is given in Table 2. The velocity diagrams at each mesh node (corresponding to the intersection of quasi-orthogonals with streamlines), in the meridional plane, are also shown in Figures 3b and 3c for the design point conditions.

For all cases studied and summarized in Table 1, the impeller passage is divided into eleven stream tubes. The inlet total pressure and temperature are kept constant at values of 42.5 lb/in^2 and 2710°R, respectively.

PRESENTATION OF RESULTS AND DISCUSSIONS

Two groups of numerical results are considered in this section. The first one deals with the flow distribution in the meridional plane of the turbine rotor. The second group investigates the effect of variation of different parameters upon the velocity distribution over the rotor blades.

Meridional (Hub-Shroud) Results

The distribution of streamlines, lines of constant relative velocity and isobars contours in the meridional plane are considered. The solutions to be presented are selected to correspond to the cases 1, 4, 6, 12, 14 and 3 of Table 1.

a. Streamlines: The projection of the mean surface streamlines on the meridional plane for the different cases studied are shown in Figure 4. The streamlines are designated by a stream-function ratio such that the value of the streamline

indicates the percentage of the flow through the turbine between the streamline and the rotor hub. The streamline spacing is, therefore, indicative of the velocity relative to the rotor, with close spacing indicating high velocities and wide spacing indicating low velocities. It is obvious that the general trend of the streamline distribution is the same for all cases studied.

b. Meridional velocity distribution: Lines of constant relative velocity to the rotor are shown in Figure 5. For the design condition corresponding to the standard solution of Table 1, the rate of acceleration along the shroud is seen to be much higher than that along the hub (case no. 1). Such behavior is similar to that of flow approaching a turning duct. As expected, this rate of acceleration along the shroud is observed to increase with the increase of mass flow rate, rotational speed and the number of impeller blades (compare cases 1, 6 and 12).

Examination of Figure 5 indicates that although the annulus cross-sectional area of the rotor increases by 73% from inlet to exit, the velocity increases generally all over the channel. This phenomenon may be attributed to the rapid decrease of density along the flow path as may be revealed from Figure 6.

Along the hub, and especially near the rotor tip, regions of decelerated flow are observed for all cases studied. The extent of these regions and the velocity gradient through each give an indication of the boundary layer behavior. This of course has serious effects on the rotor efficiency. As a general rule, it is observed that for the cases of low mass flow the negative velocity gradient along the hub is so high that regions of reversed flow do exist, as shown in case no. 12. This would result in a high level of turbulence with accompanying flow separation and mixing losses.

The present results have important significance on the process of channel design for a radial turbine, particularly when the rotor is operated at high specific speeds. In such cases, the inlet-to-exit radius ratio of the rotor is small,

moreover, the curvature of the hub is large to turn the flow from radial to axial direction. Thus a careful design of the rotor and flowpath is required to prevent flow separation from the hub.

Blade Surface Velocity Distribution

The velocity distributions over the rotor blades are considered in what follows. The examples which are presented, illustrate the effect of changing the number of blades, the mass flow rate and the impeller tip Mach number on these velocity distributions. This is followed by an investigation of the effect of changing the stator exit angles upon the performance characteristics of the rotor.

Effect of Changing Number of Blades:

Flow analyses for the 10 and 14 bladed rotors, described in Table 1, were also performed. Figures 7 and 8 compare the calculated blade surface velocity distributions for these rotors with the distribution of the basic 12 bladed rotor. At the design point (standard solution) the velocity distribution shows some diffusion on the suction side of the blades especially at turbine exit near the shroud (Fig. 7) and at the middle channel near the hub (Fig. 8). The rotor has also a leading edge separation and flow reversal over the pressure surface near the hub and between the nondimensional distance from tip ($\Delta m/m$) of 0.4 and 0.7 near the shroud.

Examination of Figures 7 and 8 show clearly that an increase in the number of rotor blades is accompanied by a reduction in blade loading. This effect is expected since the increase in number of blades reduce the blade passage effective area through which the flow passes, giving more guidance to the flow. The last figures also indicate that reducing the number of blades result in an increase in the local diffusion as well as the extent of the flow reversal regions.

It is a common practice to consider the pressure surface reversal regions as well as the suction surface diffusion as the governing parameters for rotor losses. Therefore, the

implication of the previous calculated velocity distribution is that a reduction of the number of rotor blades is accompanied by a loss of turbine efficiency. However, one should take into account that there ought to be an optimum for the total number of blades. This optimum could be defined by weighing the opposing effect of increased friction losses with (or against) benefits gained by reducing the flow reversal region as a consequence of increasing the number of blades.

Effect of Mass Flow Rate:

The effect of variation of mass flow rate upon the blade surface velocities is illustrated in Figures 9 and 10. In these figures, all design and operating conditions (other than the mass flow) were maintained constant at the standard value, (Table 1).

Figure 9 shows the calculated velocity distributions along the rotor hub at both the suction and the pressure surfaces. It is evident from this figure that the blade loading* increases as the mass flow passing through the turbine increases. Near the turbine exit section the increase in blade loading with mass flow results primarily from an increase in velocity along the suction surface.

Figure 10 shows the calculated velocity distributions along the shroud of the rotor. At low mass flow the rotor tip element is operated at an incidence angle above the design value and beyond the stall conditions as evidenced by the negative loading near the tip for the 80% mass flow case. The calculated negative velocity (in reversed flow regions) at the rotor pressure surface is noticed to be almost the same for all mass flow studied (reaching a maximum around 350 ft/sec). On the other hand, the extent of the region which the reversed flow occupies is inversely proportional to the mass flow rate. As for diffusion along the suction side, a relatively low value is obtained for the case corresponding to low mass flow.

---

* Loading is defined here as the difference between the suction surface velocity and the pressure surface velocity.

The turbine rotor has only 510 ft/sec diffusion at a mass flow rate of 80% of the design value compared to 680 ft/sec for a 100% mass flow rate. On the whole, it could be recognized from the last figures that the largest variation of impeller performance with mass flow occurred near the blade tip regions, thus indicating the criticality of design in these areas. This result has important impact on the process of blade design for new impellers, particularly when the design procedure is based on specifying the blade surface velocity distribution. The present results indicate that when high losses are expected near the inlet, the loading due to blade turning should be small since substantial losses will occur due to rapidly decelerating flow near the rotor tip.

Effect of Rotor Tip Mach Number:

The relative velocity distributions along the pressure and suction surface of the rotor blades, for different rotor tip Mach numbers are shown in Figures 11 and 12. In these figures all the design and operating conditions other than the rotational speed of the rotor were maintained constant (see Table 1). Basically, these figures indicate that a relatively high loading is initially formed near the rotor tip on both hub and shroud for low tip Mach numbers. On the other hand, as tip Mach numbers are increased, the loading near the impeller exit is observed to increase. The additional loading near the rotor tip may be attributed to the fact that the rotor is operated at a relative inlet flow angle above its design value when the rotational speed is varied. These results demonstrate once more the sensitivity of the turbine rotor performance to the variation in inlet flow angles.

As a general rule, it was observed at low r.p.m. that the velocity distribution is severely distorted. Not only the flow is reversed over a considerable portion of the pressure surfaces, but the deceleration along the suction surface is large and will lead certainly to flow separation. The present results shows that high losses are expected near the turbine inlet, when the turbine operates below the design r.p.m.

Effect of Variable Stator Angle on Turbine Performance:

In the preceding discussions, it has been demonstrated that the fluid dynamic characteristics of turbine rotors are highly sensitive to the variation in inlet flow angles. It is felt, therefore, that a detailed study of the effect of changing the stator exit angles upon the performance characteristics of the turbine will help to create a general understanding of the phenomena of rotor-stator interaction in radial machines.

Three different stator configurations are considered here to investigate the effect of stator exit angles upon the mass flow characteristics of the turbine rotor. The meridional flow field analysis of Table 2 is repeatedly performed under different operating conditions of the rotor for each stator exit angle. Figure 13 shows the variation in equivalent flow, $Q\sqrt{\theta}/\delta$, with rotational speed and pressure ratio, P_{t2}/p_3, across the rotor, for stator exit angles of 60°, 73° and 80° respectively. In drawing these characteristics, the static pressure, p_3, at exit from the rotor is evaluated on a mass-averaged basis.

Figure 13 indicates that at pressure ratio above 3 and rotational speeds below 60% of design value, the turbine is choked with a limiting flow of 0.827 lb/sec for the 73° stator exit angle. At all other conditions, for the same stator exit angle, weight flow decreases rapidly with increasing speed, indicating the impact of centrifugal effect upon the turbine rotor performance. It may be noted also that slight changes in pressure ratio have a large effect on weight flow at all rotational speeds.

Comparison of the three sets of curves of Figure 13, which correspond to different stator exit angles, shows clearly the large influence of stator exit angles upon the choking conditions in the radial machine. As a matter of fact, the choking mass flow is reduced by about a third when the stator exit angles are reduced from 80° to 63° at a rotational speed of 100% of the design value.

PART II - FLOW DISTRIBUTION AT TURBINE ROTOR EXIT

PRELIMINARY CONSIDERATIONS

Experience has shown that the shape and the geometrical configuration of the turbine exit section has a serious effect on its performance [6]. It has been common practice to design turbine rotors such that the flow leaves the machine in an axial direction. The exit section of the rotor is often designed under the assumption that the relative flow leaves the blade tangent to its trailing edge. In fact, the relative exit flow angle, β_3, at each radius of the turbine exit, usually deviates from the corresponding geometrical exit angle, β_g, (Fig. 14). Such deviation may be attributed primarily to the secondary flow effects caused by the relative swirl motion within the various blade passages due to the impeller rotation, as shown in Figure 15. An approach which has been used to determine these deviation angles is based upon the use of an empirical formula [7]. As new design concepts are developed, a need for a more comprehensive and rigorous method of predicting the deviation angles is needed. This step is critical in the design process since excessive flow angle deviations may result in flow separation with the subsequent drop in the efficiency of the expansion process.

In the following study, an analytical model which predicts the magnitude of swirl velocity behind the rotor of a radial inflow turbine is proposed. The model is based on the analytical solution of the governing equations of two dimensional irrotational flow between blades with some simplifying assumptions. The effects of variations in the following design parameters of the impeller upon the swirl velocity distribution are also investigated:

a. Hub to shroud radius ratio
b. Circumferential spacing between blades
c. Impeller rotational speed
d. Turbine flow rate.

From the analytical solution obtained, along with appropriate assumptions concerning the blade shapes, deviation angles at rotor exit are calculated. In this context, the flow angle

distribution in tangential direction, along the turbine exit section is presented for the rotor of Figure 3a under various operating conditions. Finally, possible improvements in flow nonuniformity by means of design changes using the results of the present method analysis are indicated.

ANALYSIS

Method of Approach

The method of approach taken here is to construct a calculational procedure for analyzing the flow conditions at the rotor exit. The analytical model developed for that reason is based upon the analysis of two dimensional flow between blades on the flow surface of revolution, S_m, of Figure 16. A developed view of the flow stream channel, S_m, of thickness, h, in the meridional plane, together with the coordinate system used in the analysis are also shown in the same figure. The flow field analysis procedure employed to derive the necessary governing equations used in the present study is identical to that presented in Ref. [8]. The variations in the flow properties between blades on the flow surface of revolution, S_m, is obtained through the solution of the governing equations by the method of separation of variables. The solution obtained will be used to predict the influence of the chosen blade shape (or boundary conditions) upon the relative velocity and the flow angle distribution at exit from the turbine rotor.

Governing Equations

a. Continuity:

From continuity considerations for a steady compressible flow through the stream tube of Figure 16, the following expression is obtained:

$$\frac{\partial}{\partial M}\left(\frac{\rho}{\rho_o} V H R\right) + \frac{\partial}{\partial \theta}\left(\frac{\rho}{\rho_o} U H\right) = 0 \qquad (5)$$

A nondimensional stream function, ψ, satisfies the continuity Equation (5) if defined as

$$\frac{\partial \psi}{\partial \theta} = \frac{\rho}{\rho_o} V H R \tag{5a}$$

$$\frac{\partial \psi}{\partial M} = - \frac{\rho}{\rho_o} U H \tag{5b}$$

where

$$U = \frac{W_\theta}{\omega r_s} , \qquad V = \frac{W_m}{\omega r_s} , \qquad R = \frac{r}{r_s} ,$$

$$H = \frac{h}{h_s} , \qquad M = \frac{m}{r_s} \tag{5c}$$

b. Relative Irrotational Motion

In the absence of shocks and viscous effects, the absolute motion of the fluid on the surface of revolution, S_m, is irrotational. Therefore the relative circulation is zero.

$$\Gamma = \frac{\partial}{\partial M} [R U + R^2] - \frac{\partial}{\partial \theta} [V] = 0 \tag{6}$$

Substitution of the stream function, ψ, as defined by Equation (5a) and (5b) in the above equation gives

$$2H \frac{\rho}{\rho_o} \sin\alpha = \frac{\partial^2 \psi}{\partial M^2} + \frac{1}{R^2} \frac{\partial^2 \psi}{\partial \theta^2} + \frac{\partial (\ln F)}{\partial M} \frac{\partial \psi}{\partial M}$$

$$- \frac{1}{R^2} \frac{\partial}{\partial \theta} (\ln \frac{\rho}{\rho_o}) \frac{\partial \psi}{\partial \theta} - \frac{\partial}{\partial M} [\ln (H \frac{\rho}{\rho_o})] \frac{\partial \psi}{\partial M} \tag{7}$$

where

$$\sin\alpha = \frac{dR}{dM}$$

Equation (7) is a nonlinear partial differential equation for the nondimensional stream-function distribution of two-dimensional flow past arbitrary blade shapes. For given boundary conditions, equation (7) could be solved using numerical techniques to obtain

the velocity field between blades [9]. Basically, these numerical solutions require a large amount of computation time. Therefore, it would be advantageous to have quicker means, based on some simplifying assumptions, for estimating the flow conditions between blades. With this motivation, a mathematical solution to the governing equation is considered in the next section.

Assumptions and Limitations for the Analytical Solution

To simplify the task of finding an analytical solution to equation (7), the following assumptions have been made:

a. The flow through the passage between blades is considered to be incompressible.
b. The passage height in the meridional plane is constant with radius, hence H = 1.
c. The rotating impeller has straight radial blades.
d. Variation of axisymmetric stream surface angle, α, with radius is neglected. Consequently, the flow surface of revolution is conical, and α is constant.

Under the stipulation of the foregoing, equation (7) is simplified to give

$$2 = \sin\alpha \frac{\partial^2\psi}{\partial R^2} + \frac{\sin\alpha}{R} \frac{\partial\psi}{\partial R} + \frac{1}{R^2 \sin\alpha} \frac{\partial^2\psi}{\partial\theta^2} \tag{8a}$$

also, equations (5a) and (5b) reduce to

$$V = \frac{1}{R} \frac{\partial\psi}{\partial\theta} \quad , \qquad U = - \frac{\partial\psi}{\partial R} \sin\alpha \tag{8b}$$

Equation (8a) is a Poisson equation and its solution is given by the method of separation of variables as:

$$\psi = \psi' + R(R) \tag{9}$$

where ψ' in the above equation satisfies Laplace equation, then

$$\psi = R_1(R)\ \theta(\theta) + R_2(R) \tag{10}$$

Substituting for ψ' in equation (8) one obtains:

$$\frac{\sin^2\alpha}{R_1}\left[R^2\frac{d^2R_1}{dR^2} + R\frac{dR_1}{dR}\right] + \frac{1}{\theta}\frac{\partial^2\theta}{\partial\theta^2} = 0 \tag{10a}$$

Similarly, substituting for $R_2(R)$ in equation (8) one obtains:

$$\frac{d^2R_2}{dR^2} + \frac{1}{R}\frac{dR_2}{R} - \frac{2}{\sin\alpha} = 0 \tag{10b}$$

Therefore, the expressions given by equation (10) satisfies the governing equation (8) providing the following relations are satisfied:

$$R^2\frac{d^2R_1}{dR^2} + R\frac{dR_1}{dR} + \lambda^2\frac{R_1}{\sin^2\alpha} = 0$$

$$\frac{1}{\theta}\frac{d^2\theta}{d\theta^2} - \lambda^2 = 0 \tag{11}$$

$$\frac{d^2R_2}{dR^2} + \frac{1}{R}\frac{dR_2}{R} - \frac{2}{\sin\alpha} = 0$$

where λ = constant, to be determined from boundary conditions.

After solving the set of the above given ordinary differential equations, the general solution of the stream function ψ is as follows:

$$\psi = \left[A_1\cos\left(\frac{\lambda}{\sin\alpha}\ln R\right) + A_2\sin\left(\frac{\lambda}{\sin\alpha}\ln R\right)\right]\left[C_1\sinh\lambda\theta + C_2\cosh\lambda\theta\right] + \frac{R^2}{2\sin\alpha} + D_1\ln R + D_2 \tag{12}$$

where A_1, A_2, C_1, C_2, D_1, and D_2 are constants of integration to be determined from boundary conditions.

Once the value of ψ is deduced from equation (12), the complete analysis of the theoretical velocity distribution in the rotating impeller channel is obtained using equation (8b).

If the angular spacing between two successive blades is denoted by 2σ, and the radius ratio of the hub ($= r_{hub}/r_{shroud}$) as r_1. The boundary conditions to equation (12) in the special case of a pure radial turbine, for which the blade to blade stream surface is similar to that given in Figure 16C, may be written as:

1. $\psi = 0$ at $\theta = \pm\sigma$
2. $\psi = 0$ at $R = 1$ (corresponding to shroud radius)
3. $\psi = 0$ at $R = r_1$
4. $\psi(\theta) = -\psi(\theta)$ at any radius ratio.

The first boundary condition gives:

$$C_1 = 0$$

The second boundary condition results in:

$$A_1 = 0 \qquad \text{(For Laplace equation)}$$

$$D_2 = -\frac{1}{2\sin\alpha} \qquad \text{(For Poisson equation)}$$

While the third boundary condition gives:

$$\lambda = \frac{n\pi \sin\alpha}{\ln r_1} \qquad \text{(For Laplace equation)}$$

$$D_1 = -\frac{(r_1^2 - 1)}{2\ln r_1 \sin\alpha} \qquad \text{(For Poisson equation)}$$

Hence, the expression for ψ, using the superposition principle, reduces to

$$\psi = \sum_{n=1}^{\infty} \left[A_n \sin\left(n\pi \frac{\ln R}{\ln r_1}\right) \cosh\left(\frac{n\pi \sin\alpha}{\ln r_1}\right)\theta\right] + \frac{1}{2\sin\alpha}\left[R^2 - \left(\frac{r_1^2 - 1}{\ln r_1}\right)\ln R - 1\right] \qquad (13)$$

In order to determine the coefficient (A_n) in equation (13) the first boundary condition is applied once more:

$$\therefore \sum_{n=1}^{\infty} A_n \sin\left(n\pi \frac{\ln R}{\ln r_1}\right) \cosh\left(\frac{n\pi \sin\alpha}{\ln r_1}\right)\sigma$$

$$= \frac{-1}{2\sin\alpha}\left[R^2 - \left(\frac{r_1^{\,2}-1}{\ln r_1}\right)\ln R - 1\right] \tag{14}$$

Expanding the right hand side of equation (14) in a Fourier sine series, one obtains:

$$A_n = \frac{[1-(-1)^n r_1^{\,2}]\left[\frac{1}{n} - \frac{n\pi^2}{n^2\pi^2 + 4(\ln r_1)^2}\right]}{[\pi\sin\alpha]\left[\cosh\left(\frac{n\pi \sin\alpha}{\ln r_1}\right)\sigma\right]} \tag{15}$$

The general solution for ψ may now be written as

$$\psi = \frac{1}{2\sin\alpha}\left[R^2 - \left(\frac{r_1^{\,2}-1}{\ln r_1}\right)\ln R - 1\right] + \sum_{n=1}^{\infty}[1-(-1)^n r_1^{\,2}]$$

$$\cdot\left[\frac{1}{n} - \frac{n\pi^2}{n^2\pi^2 + 4(\ln r_1)^2}\right]\left[\frac{\sin\left(\frac{n\pi \ln R}{\ln r_1}\right)}{\pi \sin\alpha}\right]\left[\frac{\cosh\left(\frac{n\pi \sin\alpha}{\ln r_1}\right)\theta}{\cosh\left(\frac{n\pi\sin\alpha}{\ln r_1}\right)\sigma}\right] \tag{16}$$

It is to be noted that this latter solution is obtained from the irrotationality condition. Then, the stream function ψ expresses the case of a displacement flow, that results from the rotation of blades in still fluid. The pure through-flow which accounts for the net discharge of the impeller is obtained in a traditional way by placing a line sink at the center of rotation of stationary blades. The nondimensional stream function for a through-flow at a volume flow rate Q may be written as

$$\bar{\psi} = - \frac{Q}{2\pi \ \omega r_s^2 \ h_s} (\theta + \sigma) \tag{17}$$

Various operating conditions may be obtained by a linear combination of solutions (16) and (17). This procedure is valid by the linearity of Laplace equation and the fact that each solution separately satisfies its own boundary condition.

ESTIMATION OF THE RELATIVE SWIRL VELOCITY DISTRIBUTION

Shown in Fig. 17 is the blade exit configuration in a typical turbine. The geometrical blade angle (β_g) is related to the minimum width of the flow passage at blade exit (o) and the blade pitch (t) at certain radius by the relation

$$\beta_g = \sin^{-1}(o/t) \tag{18}$$

In the absence of secondary flow caused by swirl motion, the relative flow at the blade exit would have a direction of β_g. When the effect of relative swirl velocity, u , is considered, the relative exit flow angle, β_3, at each radius of the turbine deviates from the corresponding geometrical angle, β_g. At the shroud, swirl motion exhibits backward characteristics because the fluid actually leaves with a slight backward component, as illustrated in Fig. 18a. At the hub, the relative swirl motion produces a forward characteristics as shown in Fig. 18b. The important effect, from the practical point of view, is that the tangential component of the absolute velocity, $C_{3\theta}$ is altered across the rotor exit in accordance with the swirl velocity distribution. Consequently, radially nonuniform exit flow conditions prevail with the subsequent redistribution of available power output at each radius of the turbine exit.

In order to obtain an accurate estimation of the net power output from a turbine for design purposes, a knowledge of the relative swirl velocity distribution at rotor exit is required.

The task of producing the necessary equation suitable for the prediction of relative swirl velocity is presented below.

Referring to Figure 18, the tangential component of swirl velocity is given by:

$$u = \omega r - W_{3\theta} \tag{19}$$

From the expression given by equations (8b), (16) and (19), the value of the nondimensional tangential component of swirl velocity, U_s, at any radius, R, will be:

$$U_s = R - \sin\alpha \frac{\partial}{\partial R} [\psi + \bar{\psi}]$$

$$= \frac{1}{2R}\left(\frac{r_1^2 - 1}{\ln r_1}\right) - \sum_{n=1}^{\infty} \left[\frac{\tau}{\pi} \frac{\lambda}{R\sin\alpha} \cos\left(\frac{\lambda \ln R}{\sin\alpha}\right) \frac{\cosh(\lambda\theta)}{\cosh(\lambda\sigma)}\right] \tag{20}$$

where

$$U_s = \frac{u}{\omega r_s} \quad , \quad \lambda = \frac{n\pi \sin\alpha}{\ln r_1} \quad , \sigma = \frac{\pi}{z}$$

$$\tau = [1-(1)^n r_1^2]\left[\frac{1}{n} - \frac{n\pi^2}{n^2\pi^2 + 4(\ln r_1)^2}\right] \tag{20a}$$

The theoretical distribution of (U_s) as given by equation (20) is seen to depend primarily upon the following parameters:

1. Number of blades.
2. Hub to shroud radius ratio, r_1.
3. The radius (R) and position (θ) at which swirl velocity is evaluated.
4. Axisymmetric stream surface angle, α, independent of the turbine flow rate.

Variation of U_s with these parameters will be studied in the next section, for the special case of a radial inflow turbine in which, $\alpha = \pi/2$.

IV. RESULTS AND DISCUSSION

Two groups of numerical examples are worked out using the present method of analysis. The first one investigates the effect of number of blades and hub-to-shroud radius ratio on the swirl velocity distribution at turbine exit. The second group deals with the influence of the same parameters in addition to the effect of mass flow rate and the impeller rotational speed on the flow angle distribution at rotor exit.

Passage-Averaged Value of Swirl Velocity Distribution at Turbine Exit

Calculations which give an indication of the magnitude of the tangential component of swirl velocity, U_s, at turbine exit are performed using the first ten terms of the series in equation (20). Higher order terms have been neglected. Sample results showed that the maximum error introduced by such approximations lie within 0.2% as compared with those calculated using up to fifty terms. The value of U_s from blade-to-blade at different angular positions, θ, are averaged over the blade passage at each radius ratio, R. The variation of this average value, $\bar{U}_s$, near the hub is plotted in Figure 19 as function of hub to shroud radius ratio, r_1, with the number of impeller blades, Z, as a parameter. Absolute value of the swirl velocity, $\bar{U}_s$, is seen to decrease considerably as the number of blades is increased for all values of r_1. These curves also indicate that for a given number of blades, Z, increasing the hub to shroud radius ratio, increases the absolute value of $\bar{U}_s$ until a maximum is reached. The points of maxima are shifted towards lower values of r_1 as the number of blades decreases.

Figure 20 shows the variation of $\bar{U}_s$ near the shroud. Unlike the previous case, it is obvious that for a given number of blades, there exists a region of relatively constant $\bar{U}_s$, and a region of changing $\bar{U}_s$. The region of constancy extends over a large portion of radius ratio r_1, and its extent increases

as the number of blades increases. Accordingly, a reduction in the absolute value of $\bar{U}_s$ at the shroud is achieved only by selecting higher design values of hub-to-shroud radius ratio.

The effect of variation of both the hub-to-shroud radius ratio, r_1, and the angular spacing between blades, σ, upon the swirl velocity distribution at turbine exit is illustrated in Figures 21 through 23.

Figure 21 shows the radial distribution of the mean value of $\bar{U}_s$ over the exit section of the bladed impeller having different design values of r_1. It is evident from this figure that the hub-to-shroud radius ratio has a serious effect on the $\bar{U}_s$ distribution. For low values of r_1, the distribution obtained is nonlinear from hub to mid radius approximately. However, the distribution becomes generally linear from hub to shroud as the radius ratio approaches 0.7. Figure 21 also shows that the center of rotation of the swirl motion in an impeller having r_1 equal to 0.2 occurs at R = 0.735, and for a 0.7 radius ratio impeller at 0.845. This indicates that the radius of rotation of fluid decreases as the hub to shroud radius ratio of the impeller decreases.

The effect of changing the angular blade spacing, 2σ, (by varying the number of blades) on the radial distribution of $\bar{U}_s$ is shown for the case of a 6 and a 10 bladed impeller in Figures 22 and 23 respectively. The variation of $\bar{U}_s$ with R exhibits the same trends as discussed for Figure 21. However, the magnitude of swirl velocity, $\bar{U}_s$, is decreased by increasing the number of blades.

The impact of increasing the number of blades, Z, upon the position of center of rotation of fluid at turbine exit is also shown in Figure 23. It is evident from these figures that the center of rotation shifts towards the shroud as the number of blades is increased.

Flow Angle Distribution at Rotor Exit

In studying the effect of swirl velocity, $\bar{U}_s$, upon the relative exit flow angle, β_3, from the turbine rotor, both the flow coefficient, ϕ, and the geometrical angle distribution, β_g, at turbine exit have to be known. The flow coefficient is related to the meridional component of absolute velocity, C_3 , of Figure 18 by

$$\phi = \frac{C_3}{\omega r_{shroud}}$$

and is directly proportional to the flow rate passing through the rotor. Representative values of ϕ used in the present study are chosen to correspond to the Cases 1, 2, 3. 7, 8 given in Table 1. The relation between impeller exit radius and geometric exit angles used to carry out the necessary calculations is shown in Figure 24.

Sample results showing the influence of swirl velocity upon the distribution of relative exit flow angles are shown in Figures 25 and 26. These figures indicate clearly that the flow loses the directional influence of the blade surface for a finite number of blades.

For a given impeller geometry, the difference between β_3 and β_g depends upon the relative magnitude of the mass flow rate and the impeller rotational speed. These results indicate that for high specific speed, rotors, as in the case of small radial turbine, large deviation angles* can occur even for sizable values of the flow rate.

---

* Deviation angles are defined here as the difference between relative exit flow angle, β_3, and the corresponding geometrical angle ($\Delta = \beta_3 - \beta_g$)

For all cases studied, a positive deviation of flow angles over the geometrical angles are observed near hub, while the flow near the tip tends to have locally negative deviation angles. This implies that near the hub, separation of flow is liable to occur at blade suction surface, on the other hand near the impeller tip separation may take place at blade pressure surface. This conclusion conforms with the experimental work presented in reference [10].

The effect of increasing the number of blades is to decrease the predicted deviation at all radii, Fig. 26. The position of maximum deviation is seen to occur near hub for low mass flow, while it shifts towards the shroud for high mass flow rates, Fig. 25.

Briefly, it may be concluded that the effect of swirl velocity, $\bar{U}_s$, is to produce a non-symmetrical deviation angles distribution at rotor exit. The deviation angles at all radii may be reduced by increasing the flow rate, decreasing the impeller rotational speed, decreasing the angular blade spacing and choosing an optimum hub-to-shroud radius ratio.

It is obvious that in order to overcome the adverse effects of non-uniform flow conditions at turbine exit, procedures with which the effects of appropriate countermeasures can be estimated must be available. It is felt that with the present theoretical model such estimation can be adequately accomplished.

REFERENCES

1. Wood, Homer J., "Current Technology of Radial Inflow Turbines for Compressible Fluids," Trans. ASME, January 1963, p. 12.
2. Wallace, F.J., "Theoretical Assessment of the Performance Characteristics of Inward Radial Flow Turbines," Proc. Inst. Mech. Engrs., 1958, pp. 172, 931.
3. Katsanis, T., "Use of Arbitrary Quasi-Orthogonals for Calculating Flow Distribution in the Meridional Plane of a Turbomachine," NASA TN D-2546, 1964.
4. Stantiz, J.D. and Prian, V.D., "A Papid Approximation Method for Determining Velocity Distribution on Impeller of Centrifugal Compressors," NACA TN 2421, 1951.
5. Wu, Chung-Hua, "A General Theory of Three Dimensional Flow in Turbomachines of Axial, Radial, and Mixed Flow Types," NACA TN 2604, January 1952.
6. UACL Engineering Report No. 458, "Phase III Interim Report No. 6, 90 Degree Inward Radial Turbine Research Program," Project P3.
7. Mizumachi, T. and Kitano, M., "Study of Aerodynamic Characteristics of Rotating Blades in a Radial Inflow Turbine," paper presented at Tokyo International Conference, Oct. 4-8, 1971.
8. Vavra, M., "Aerothermodynamics and Fluid Flow in Turbomachinery," John Wiley, New York, 1960.
9. Katsanis, T., "Computer Program for Calculating Velocities and Streamlines on a Blade-to-Blade Stream Surface of a Turbomachine," NASA TND-4525, 1968.
10. Lakshminarayana, B., "Three Dimensional Flow Field in Rocket Pump Inducers," Transactions of the ASME, Journal of Fluids Engineering, December 1973, pp. 567-577.

NOMENCLATURE

Symbol	
A_1, A_2, A_n, C_1 C_2, D_1, D_2	Constants of integration in equations (11) and (14).
C	Absolute fluid velocity, ft/sec.
h	Stream channel thickness normal to meridional stream surface, ft., or static enthalpy, ft.lb./slug
H	Normalized stream-channel thickness defined as h/h_s
m	Distance along meridional stream surface, ft.
M	Normalized meridional stream line distance defined as m/r_s
O	Throat dimension, ft.
P_t	Total pressure, lb/in^2
Q	Mass flow passing through the turbine, lb/sec.
r	Radius from axis of rotation, ft.
R	Normalized radius ratio, defined as r/r_s
S	Distance along arbitrary quasi-orthogonal in meridional plane
t_θ	Blade thickness in tangential direction
u	Tangential component of swirl velocity, ft/sec.
U	Normalized tangential component of fluid relative velocity, defined as $W_\theta/\omega r_s$
U_s	Normalized tangential component of swirl velocity, defined as $u/\omega r_s$
V	Normalized meridional component of fluid relative velocity, defined as $W_m/\omega r_s$
W	Fluid velocity relative to blade, ft/sec.
Y	Prerotation in equation (1), $ft^2/sec.$
z	Axial coordinate

Z	Number of blades
α	Angle between meridional stream line and axis of rotation, deg.
β	Angle between relative velocity vector and meridional plane, radians
Γ	Circulation
δ	Ratio of turbine inlet total pressure to atmosphere pressu
θ	Relative angular coordinate, deg.
λ	Coefficient in equation (11)
ρ	Mass density, slugs/cu.ft.
ϕ	Flow coefficient at rotor exit, defined as $C_{3m}/\omega r_s$
ψ	Normalized stream function
ρ	Density, lb/ft^3
2σ	Angular blade spacing defined as $(2\pi/Z)$
ω	Rotational speed of the impeller, rad/sec.

Subscripts

2	Inlet to rotor
3	Exit from rotor
o	Total conditions
g	Geometrical
s	Shroud
θ, r, m, x	Components of argument in tangential, radial, meridional, and axial directions, respectively.

Superscripts

-	Mean value

TABLE 1

PARAMETERS FOR NUMERICAL SOLUTIONS

Solution	No. of blades	Nozzle angle (degree)	Mass flow rate (% of design)	Rotational speed (% of design)	Rotor inlet relative swirl angle, β_2	Prewhirl at rotor inlet, ft^2/sec	Pemarks
1	12	73	100%	100%	-40.91	346.98	Standard
2	10	73	100%	100%	-40.91	346.98	
3	14	73	100%	100%	-40.91	346.98	
4	12	73	100%	120%	-61.93	346.98	
5	12	73	100%	80%	- 2.2361	346.98	
6	12	73	100%	60%	38.25	346.98	
7	12	73	90%	100%	-59.61	288.49	
8	12	73	80%	100%	-69.47	241.59	
9	12	60	160%	100%	-38.54	300.62	
10	12	60	160%	80%	-16.22	300.62	
11	12	60	160%	60%	12.12	300.62	
12	12	80	65%	100%	28.60	485.61	
13	12	80	65%	80%	57.51	485.61	
14	12	80	65%	60%	68.93	485.61	

TABLE 2: INPUT CARD LISTING

ORIGINAL PAGE IS OF POOR QUALITY

a) Inlet Flow Conditions and Rotor Geometry Data:

10	11	17	13	8360.6602	0.9320	14.0000	1.3300	1715.0000
0	0	0	0	2710.0000	346.9805	0.0424	0.0010	2.5000
13	1	2	1	1.0000	-1.0000	-40.9118	1.8900	0.1000
0.00001								
0.5000		0.5250		0.5750	0.6500	0.7250	0.8125	0.8875
0.9875		1.0625		1.1625				
0.0		0.0093		0.0250	0.0750	0.1625	0.2625	0.4125
0.5875		0.8750		1.1250				
2.7400		2.6250		2.5000	2.3625	2.2500	2.1750	2.1125
2.0750		2.0500		2.0375				
2.7400		2.5000		2.2500	1.8750	1.5500	1.3000	1.0250
0.8125		0.5875		0.5000				
0.0		0.0		0.0	-0.0004	-0.0027	-0.0090	-0.0240
-0.0517		-0.0972		-0.1632	-0.2487	-0.3512	-0.4660	

b) Blade Thickness Table:

0.0	0.1000	0.2000	0.3000	0.4000	0.5000	0.6000
0.7000	0.8000	0.9000	1.0000	1.1000	1.2000	
0.3850	0.3580	0.3220	0.2900	0.2600	0.2300	0.2010
0.1750	0.1500	0.1280	0.1080	0.0920	0.0790	
0.3750	0.3450	0.3110	0.2800	0.2500	0.2200	0.1910
0.1650	0.1400	0.1190	0.1000	0.0840	0.0740	
0.3650	0.3330	0.3000	0.2700	0.2400	0.2100	0.1810
0.1550	0.1310	0.1100	0.0920	0.0780	0.0690	
0.3550	0.3210	0.2900	0.2590	0.2290	0.2000	0.1710
0.1460	0.1210	0.1010	0.0850	0.0730	0.0640	
0.3450	0.3100	0.2800	0.2490	0.2190	0.1890	0.1610
0.1360	0.1130	0.0930	0.0790	0.0690	0.0590	
0.3330	0.3000	0.2690	0.2380	0.2080	0.1790	0.1500
0.1270	0.1040	0.0860	0.0730	0.0630	0.0560	
0.3200	0.2900	0.2580	0.2270	0.1970	0.1680	0.1400
0.1170	0.0950	0.0780	0.0680	0.0590	0.0520	
0.3100	0.2790	0.2470	0.2150	0.1860	0.1570	0.1300
0.1070	0.0870	0.0730	0.0620	0.0550	0.0490	
0.3000	0.2680	0.2360	0.2040	0.1750	0.1470	0.1200
0.0980	0.0790	0.0680	0.0580	0.0510	0.0460	

Blade Thickness Table (Continued):

0.2800	0.2570	0.2240	0.1930	0.1640	0.1360	0.1100
0.0880	0.0730	0.0620	0.0540	0.0470	0.0430	
0.2510	0.2460	0.2130	0.1820	0.1530	0.1240	0.1000
0.0790	0.0670	0.0570	0.0500	0.0450	0.0400	
0.2230	0.2230	0.2020	0.1700	0.1410	0.1130	0.0890
0.0700	0.0610	0.0520	0.0460	0.0430	0.0370	
0.1940	0.1940	0.1900	0.1590	0.1300	0.1020	0.0790
0.0600	0.0500	0.0400	0.0300	0.0200	0.0100	
0.1660	0.1660	0.1660	0.1480	0.1180	0.0910	0.0690
0.0500	0.0400	0.0300	0.0200	0.0100	0.0	
0.1370	0.1370	0.1370	0.1370	0.1060	0.0800	0.0590
0.0400	0.0300	0.0200	0.0100	0.0	0.0	
0.1090	0.1090	0.1090	0.1090	0.0930	0.0700	0.0500
0.0300	0.0200	0.0100	0.0	0.0	0.0	
0.0800	0.0800	0.0800	0.0800	0.0800	0.0600	0.0400
0.0200	0.0100	0.0	0.0	0.0	0.0	
0.0	0.1000	0.2000	0.3000	0.4000	0.5000	0.6000
0.7000	0.8000	0.9000	1.0000	1.1000	1.2000	
0.5000	0.6400	0.7800	0.9200	1.0600	1.2000	1.3400
1.4800	1.6200	1.7600	1.9000	2.0400	2.1800	2.3200
2.4600	2.6000	2.7400				

ORIGINAL PAGE IS
OF POOR QUALITY

ORIGINAL PAGE IS
OF POOR QUALITY

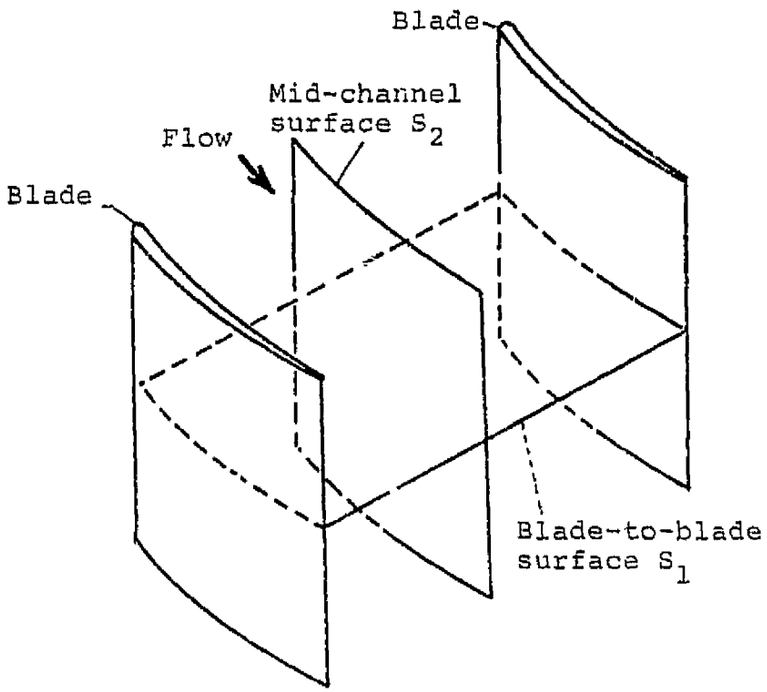

FIGURE 1. TWO-DIMENSIONAL ANALYSIS SURFACES IN A TURBOMACHINE.

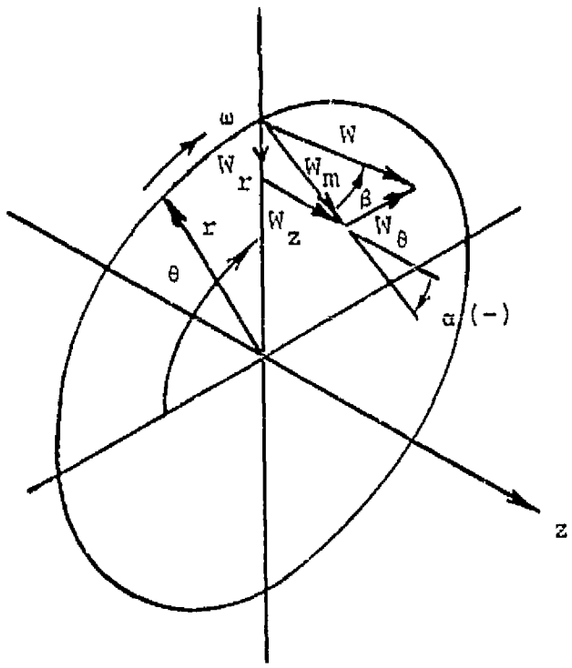

FIGURE 2. COORDINATE SYSTEM AND VELOCITY COMPONENTS.

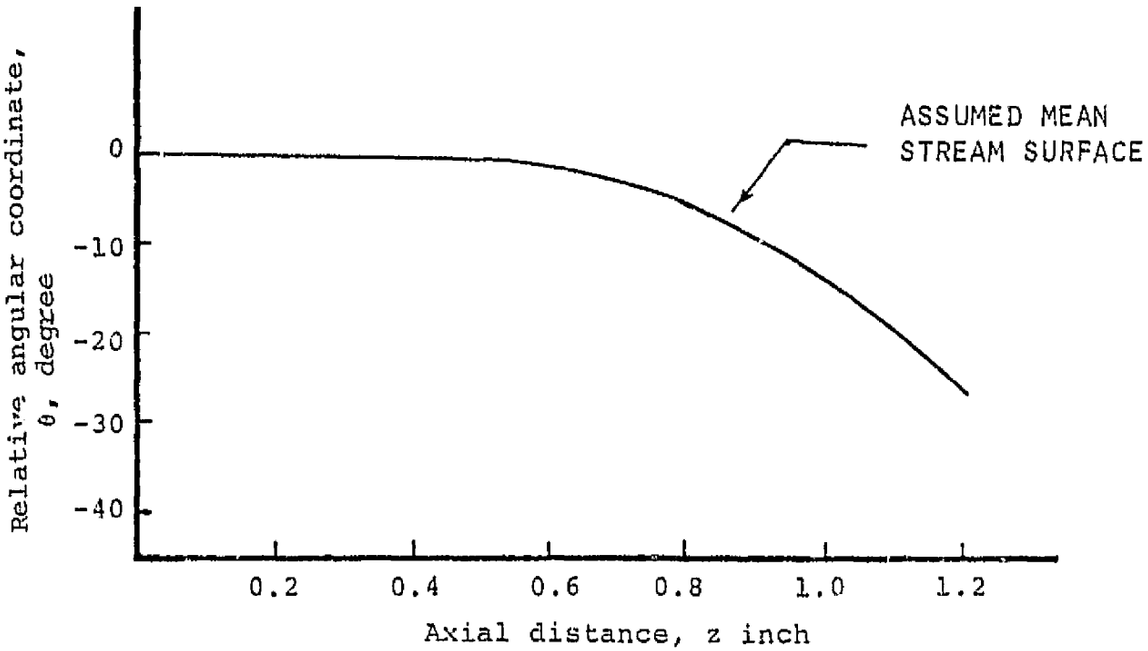

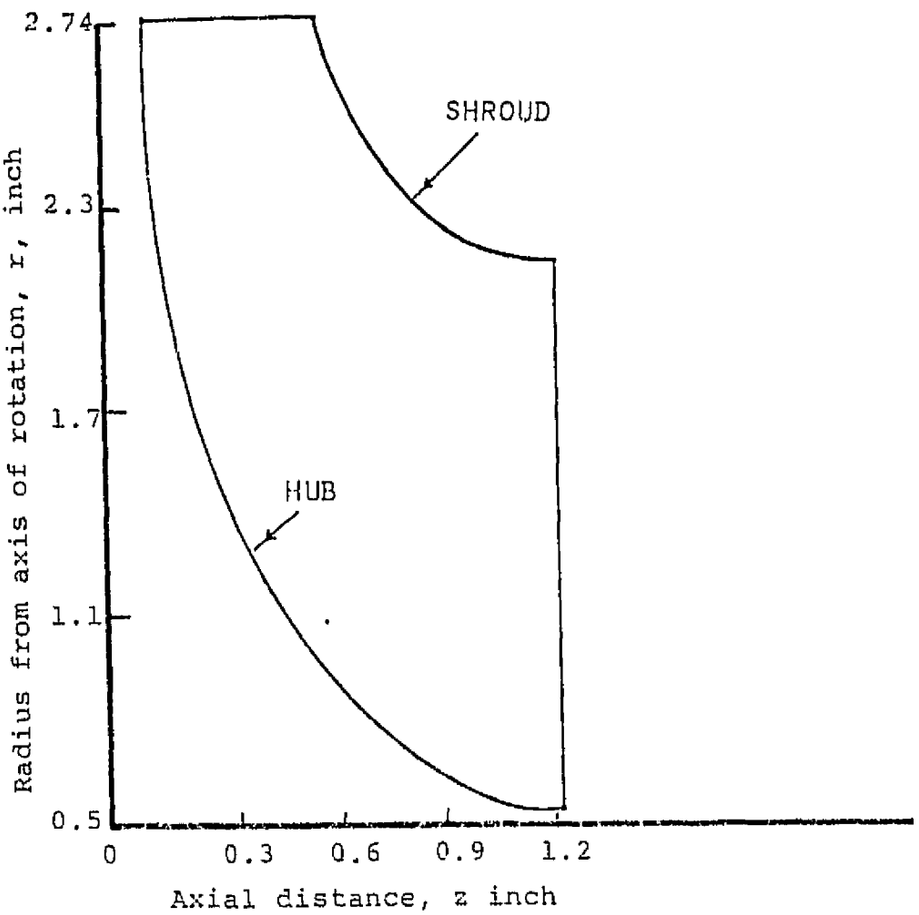

FIGURE 3A. MERIDIONAL VIEW OF THE ROTOR.

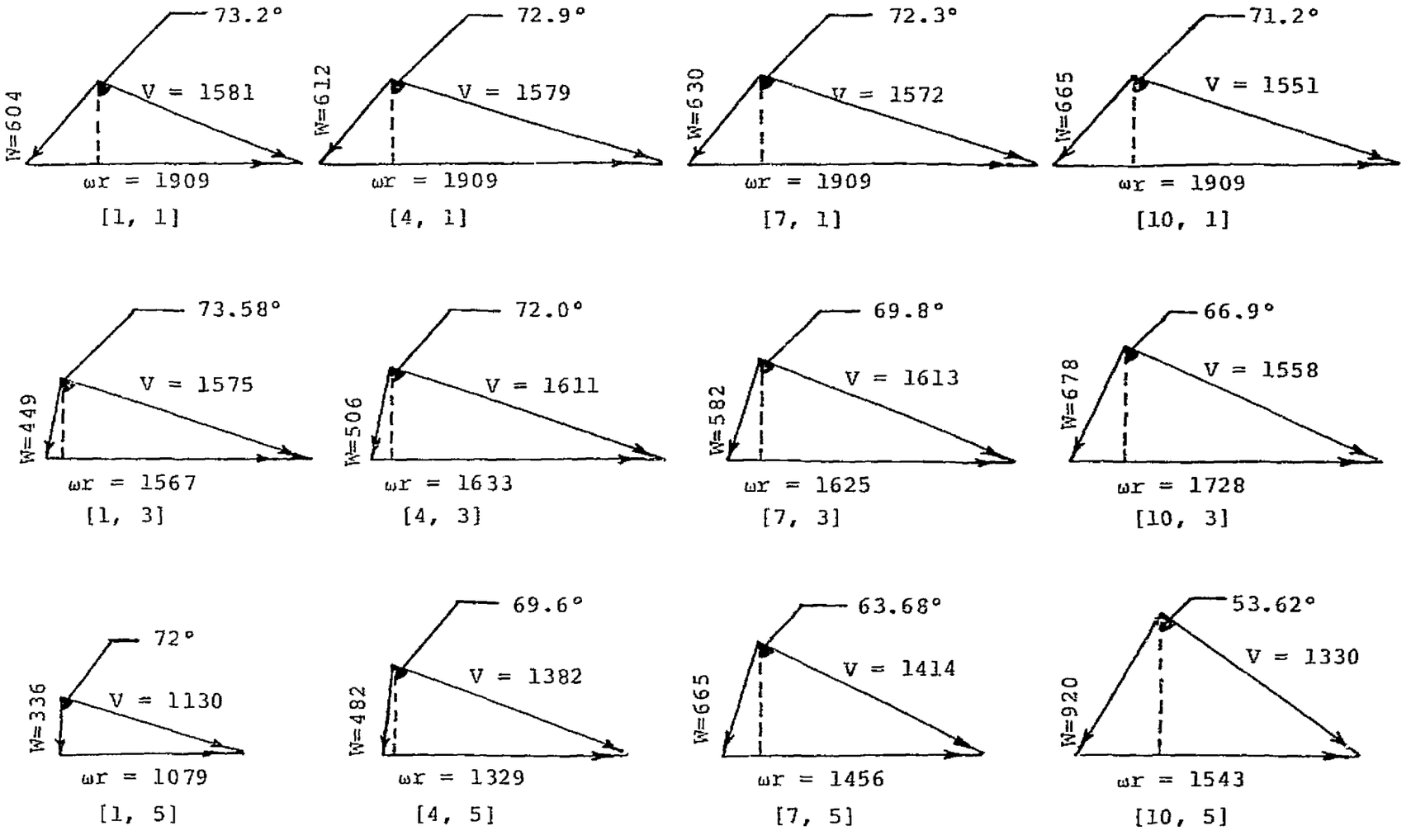

† Numbers between brackets designate the mesh location, as specified in Fig. 3d.

FIG. 3B. VELOCITY DIAGRAMS (FT/SEC), AT DIFFERENT MESHES.

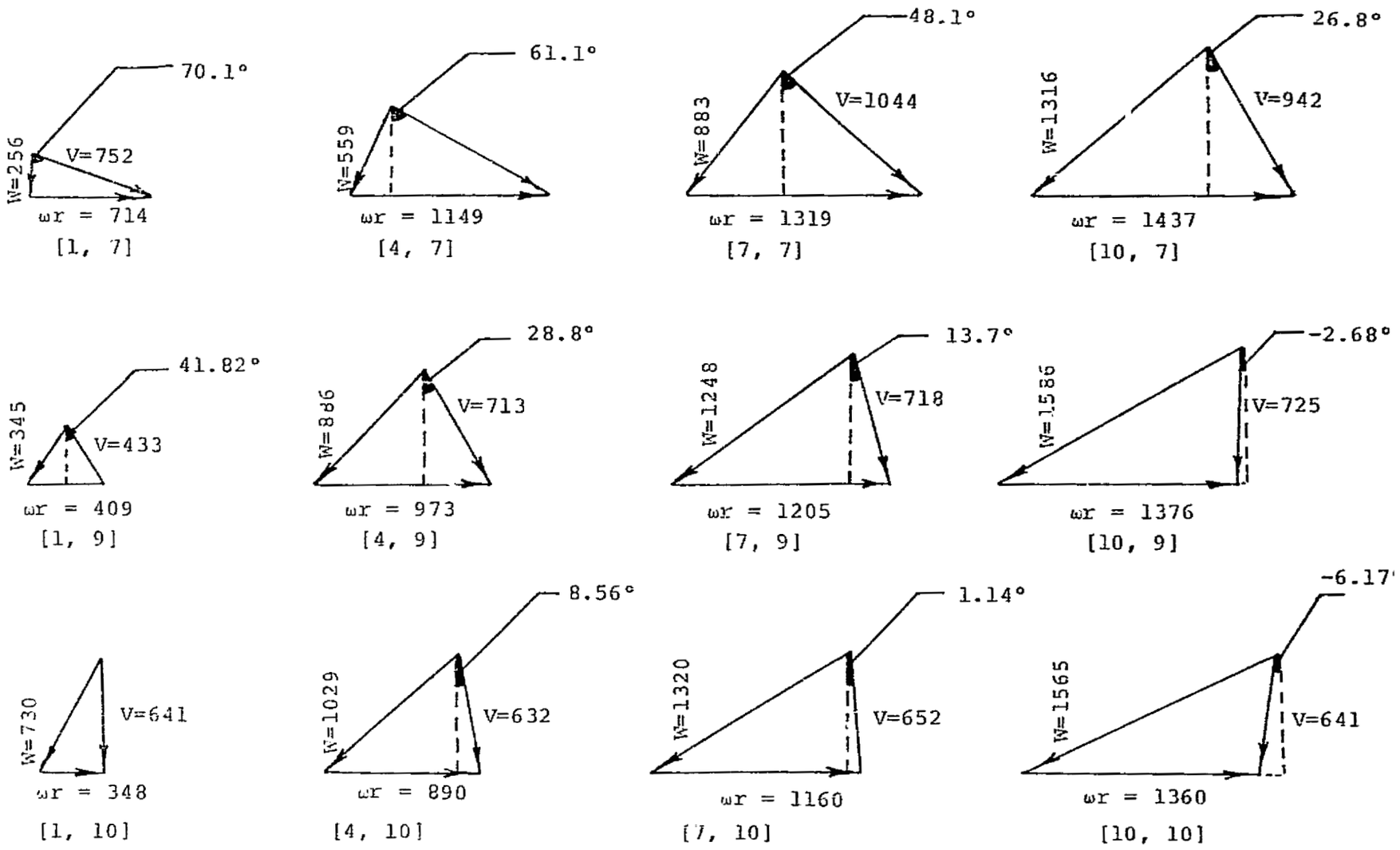

+ Numbers between brackets designate the mesh location, as specified in Fig. 3d.

FIG. 3c. VELOCITY DIAGRAMS (FT/SEC), AT DIFFERENT MESHES.

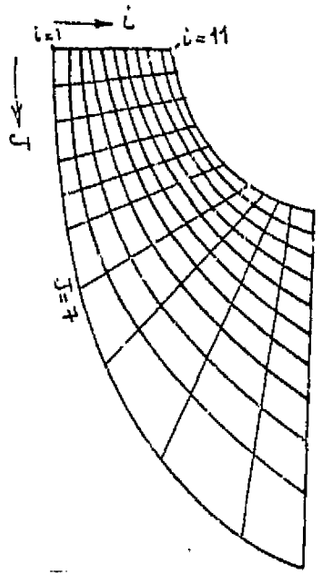

ORIGINAL PAGE IS
OF POOR QUALITY

FIG. 3D. MESH COORDINATES

Mesh Location [I, J]	Radial Coordinate r, inch	Axial Coordinate z, inch	Mesh Location [I, J]	Radial Coordinate r, inch	Axial Coordinate z, inch
[1, 1]	2.740	0.0	[1, 7]	1.025	0.4125
[4, 1]	2.740	0.153	[4, 7]	1.651	0.685
[7, 1]	2.740	0.305	[7, 7]	1.894	0.792
[10, 1]	2.740	0.452	[10, 7]	2.063	0.866
[1, 3]	2.250	0.025	[1, 9]	0.587	0.875
[4, 3]	2.344	0.232	[4, 9]	1.397	0.978
[7, 3]	2.419	0.397	[7, 9]	1.731	1.021
[10, 3]	2.481	0.533	[10, 9]	1.976	1.053
[1, 5]	1.549	0.162	[1, 10]	0.500	1.125
[4, 5]	1.908	0.451	[4, 10]	1.278	1.143
[7, 5]	2.091	0.596	[7, 10]	1.665	1.153
[10, 5]	2.215	0.697	[10, 10]	1.950	1.161

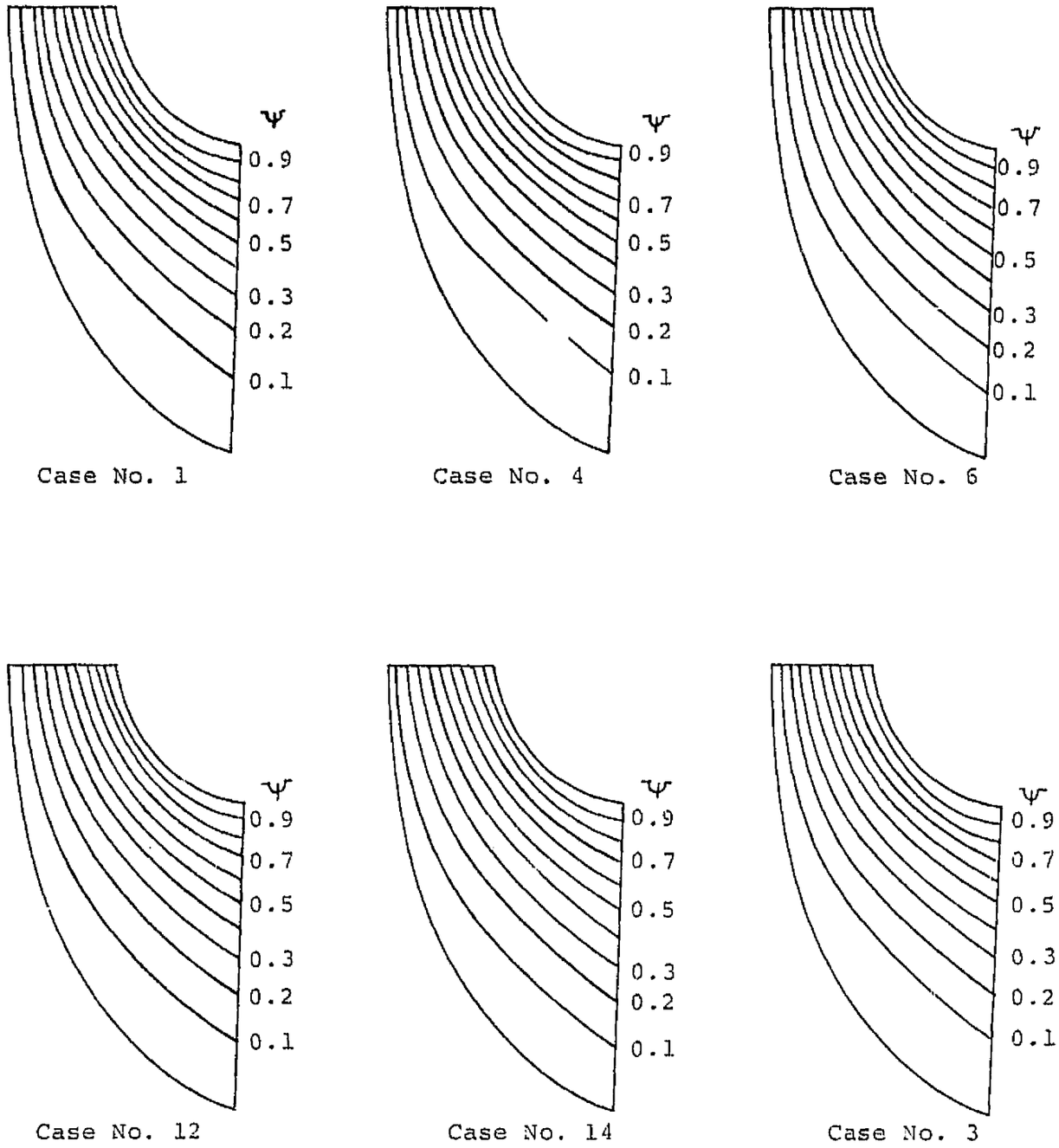

FIG. 4. STREAMLINE DISTRIBUTION IN THE MERIDIONAL PLANE.

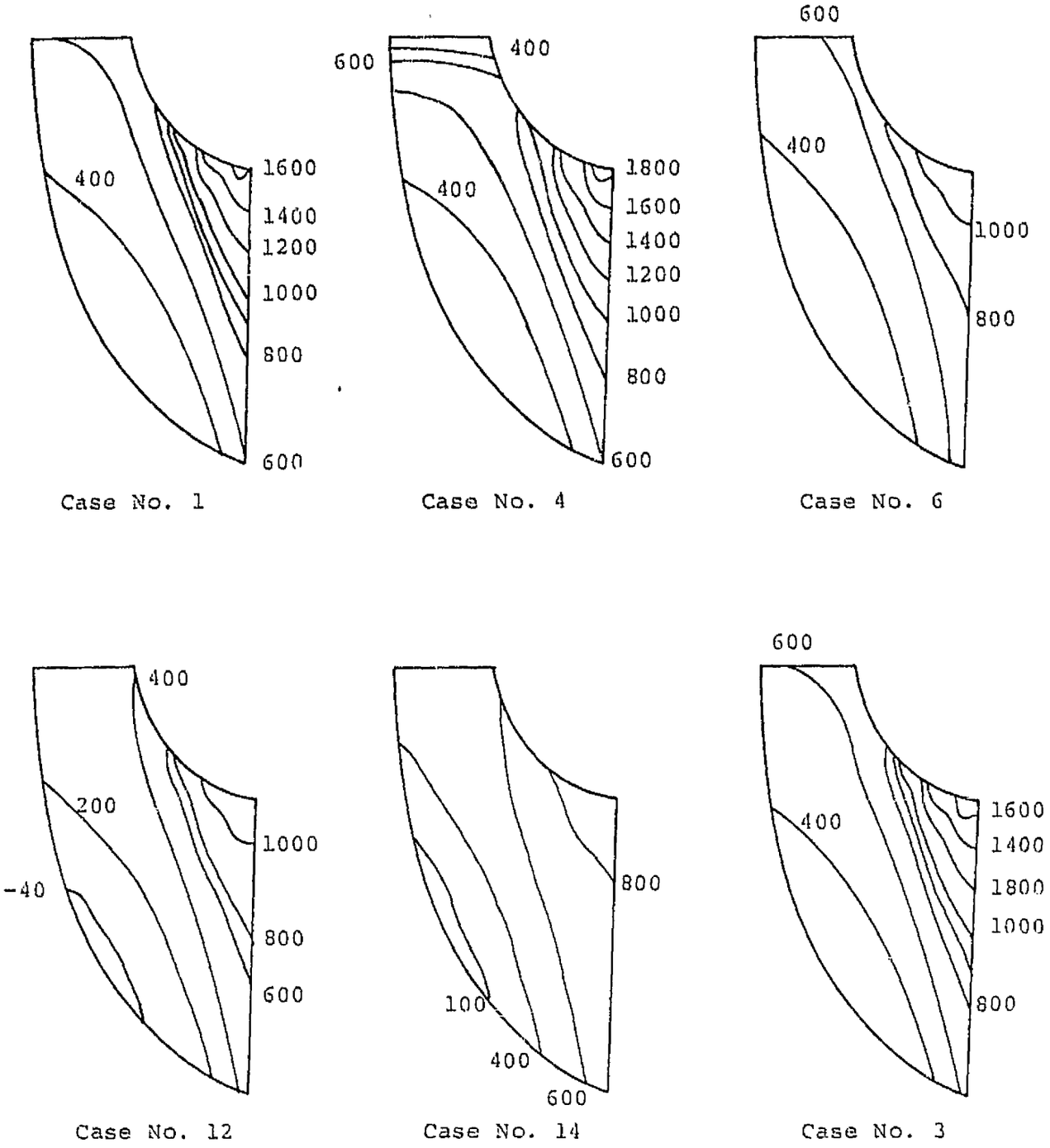

FIG. 5. MERIDIONAL VELOCITY DISTRIBUTION (FT/SEC)

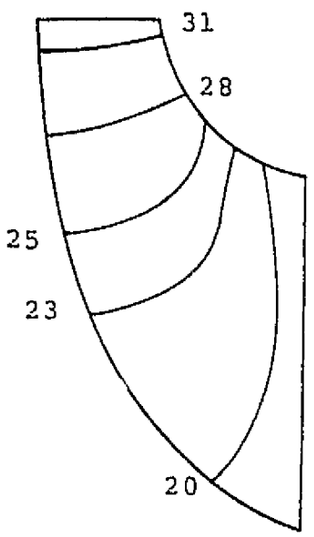

Case No. 1

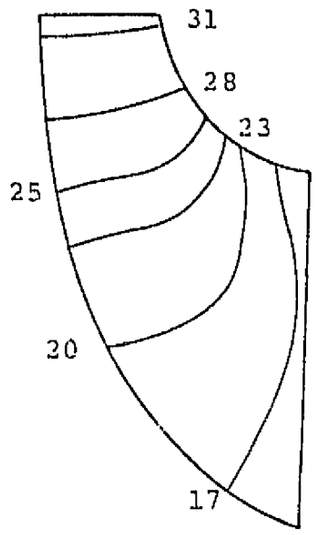

Case No. 4

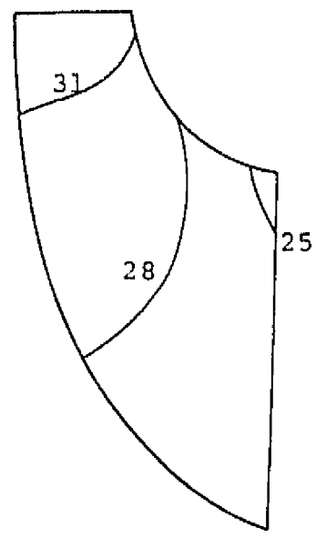

Case No. 6

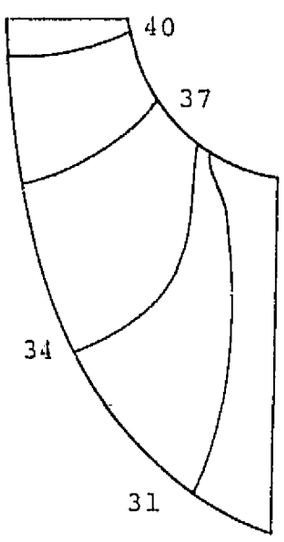

Case No. 12

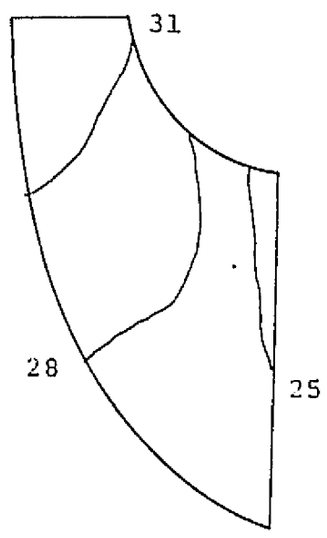

Case No. 14

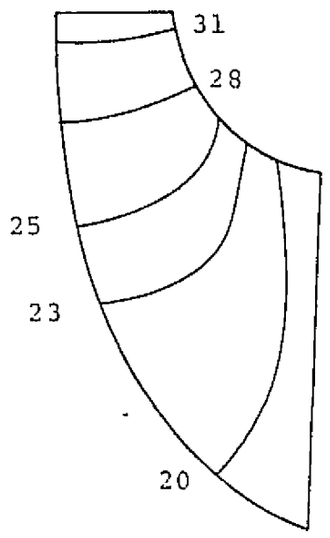

Case No. 3

FIG. 6. STATIC PRESSURE DISTRIBUTION (LB/INCH^2)

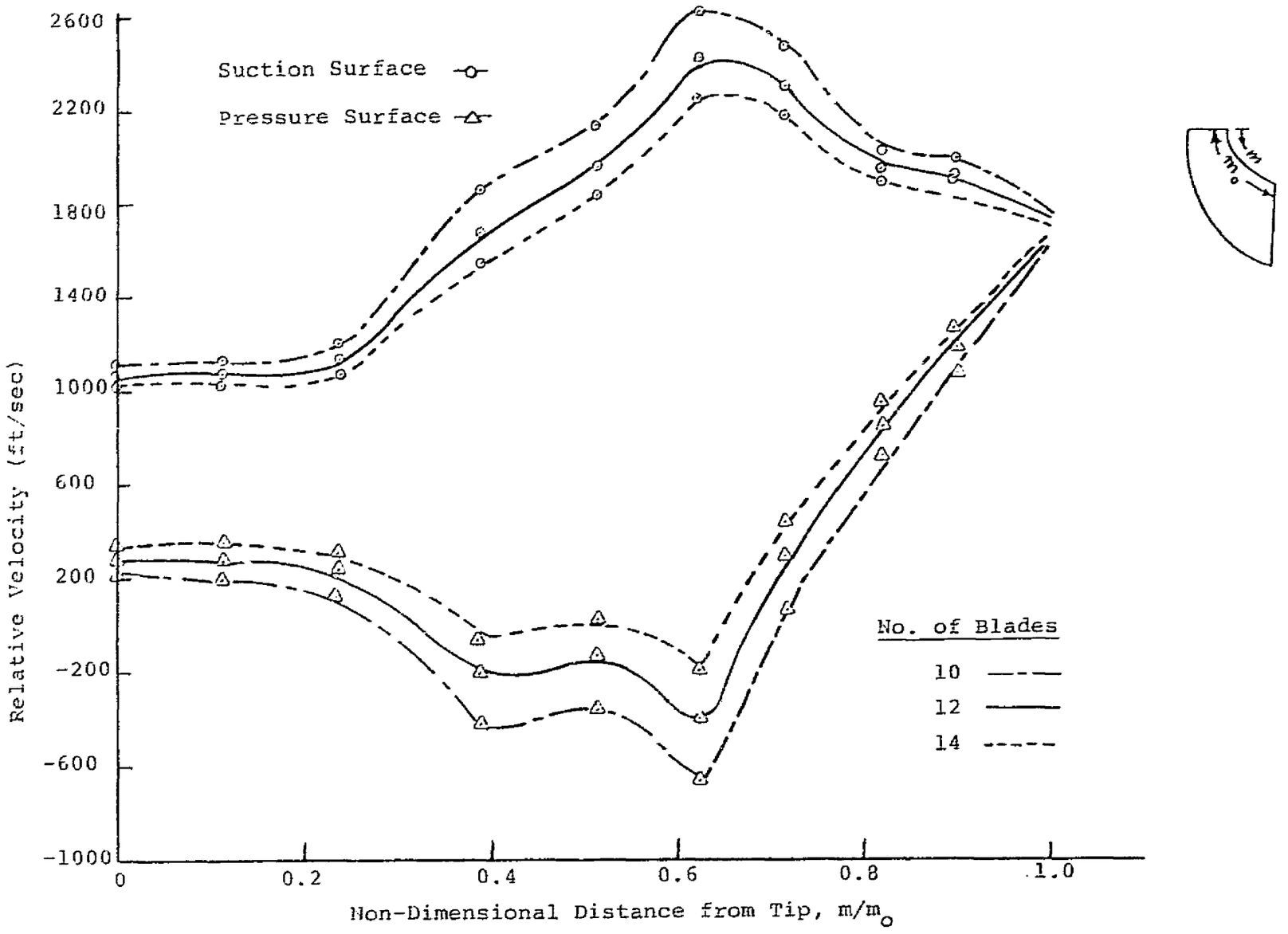

FIGURE 7. VELOCITY DISTRIBUTION NEAR SHROUD.

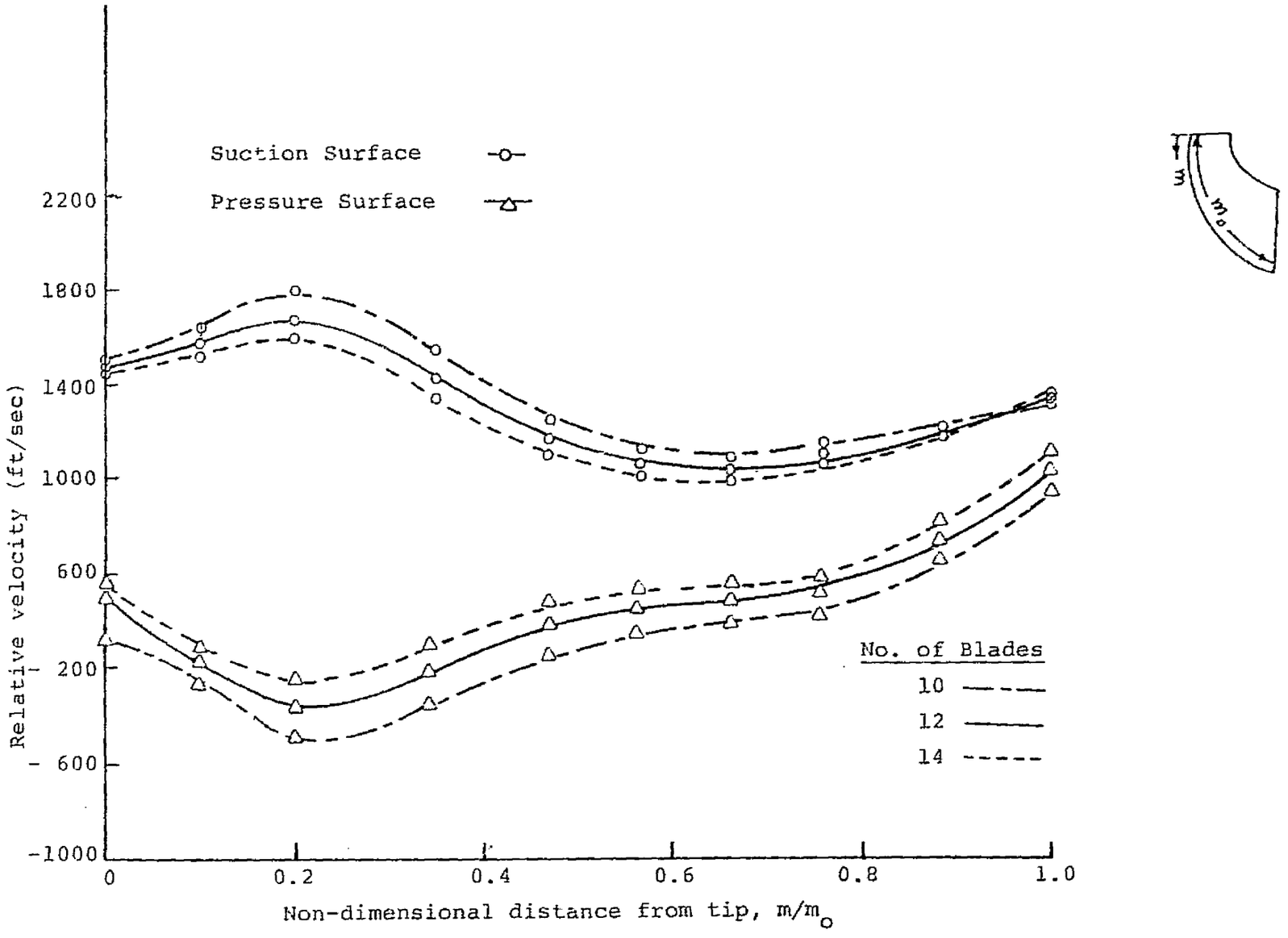

FIGURE 8. VELOCITY DISTRIBUTION NEAR HUB.

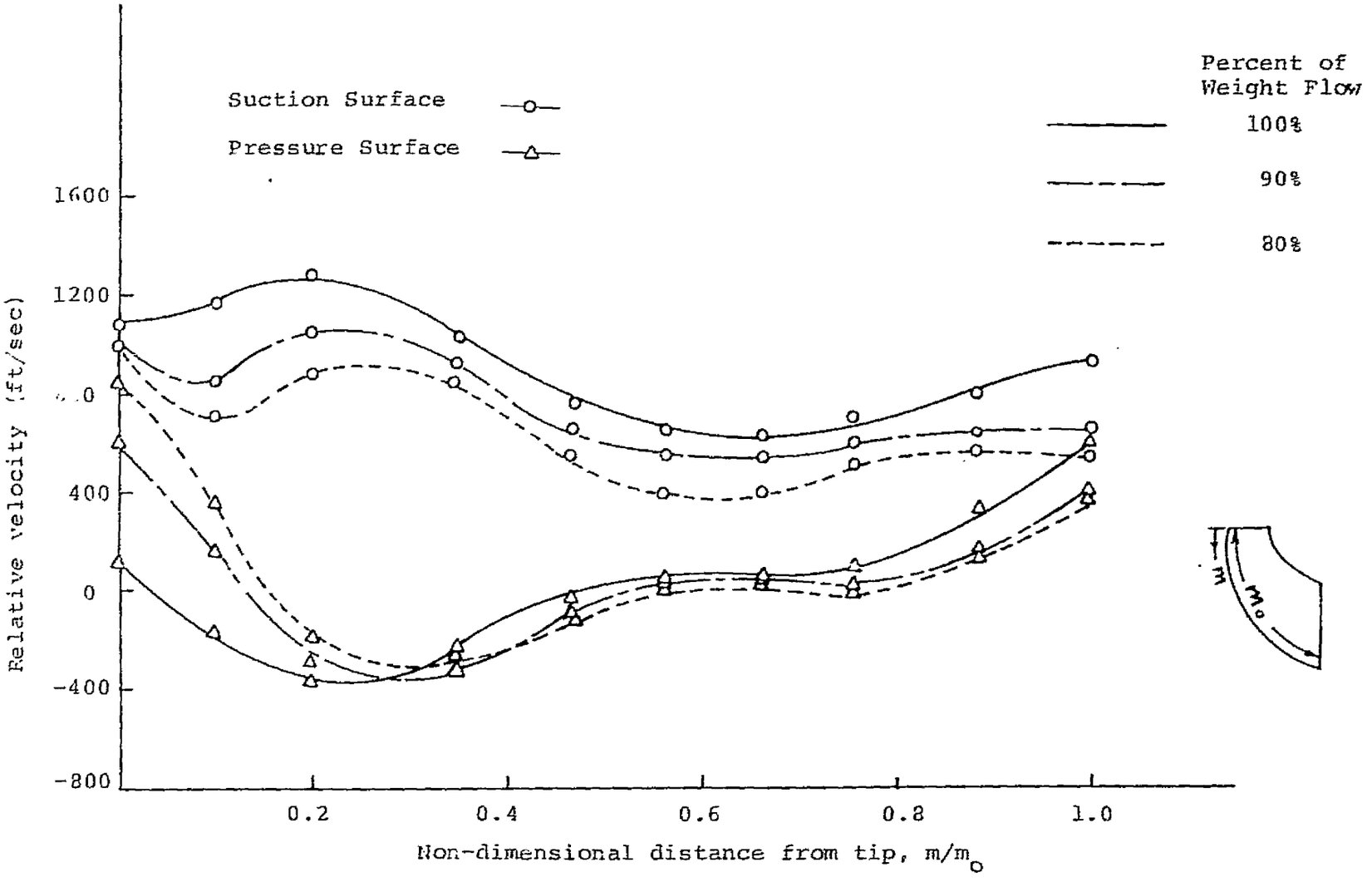

FIG. 9. VELOCITY DISTRIBUTION NEAR HUB.

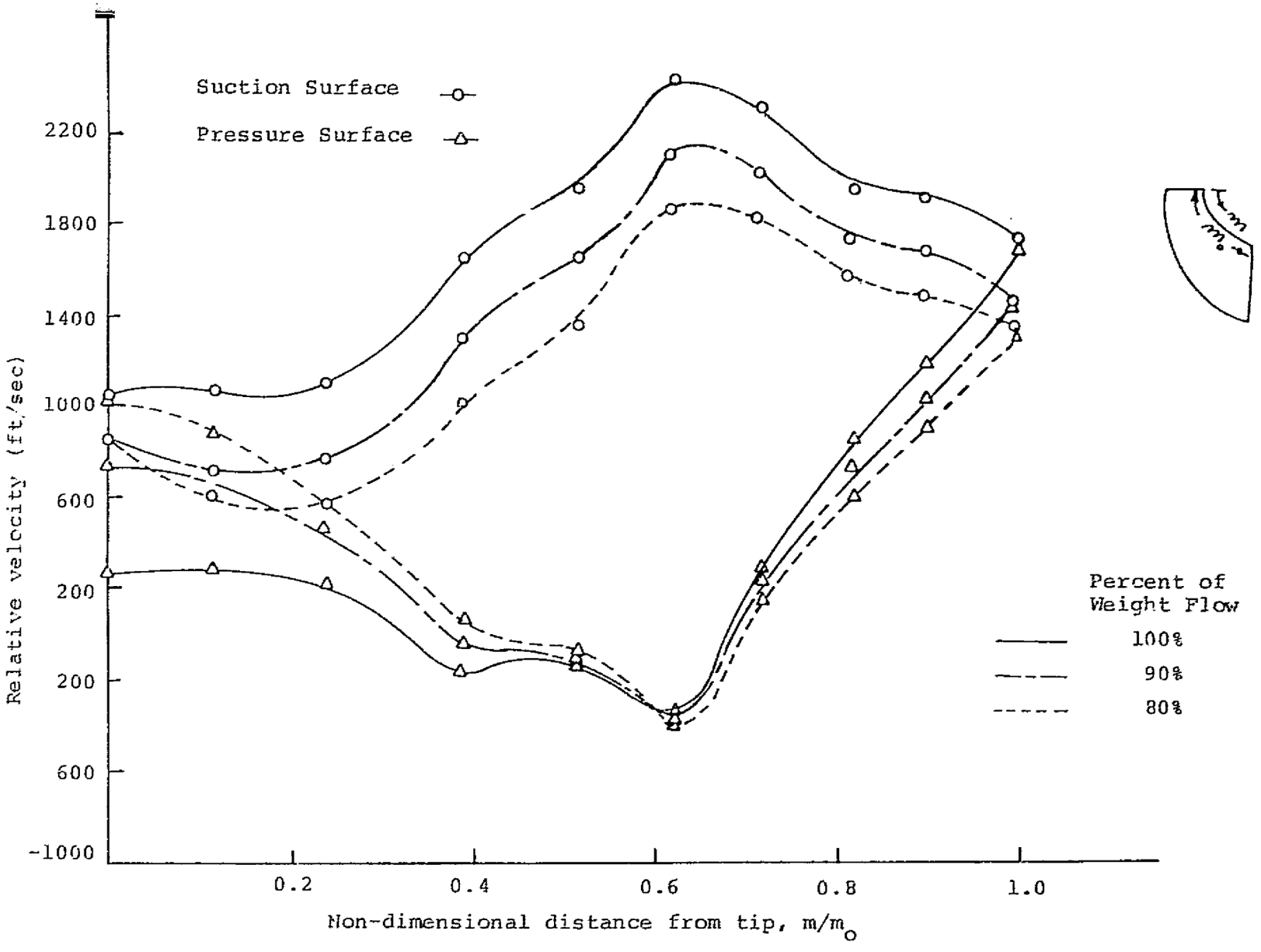

FIG. 10. VELOCITY DISTRIBUTION NEAR SHROUD.

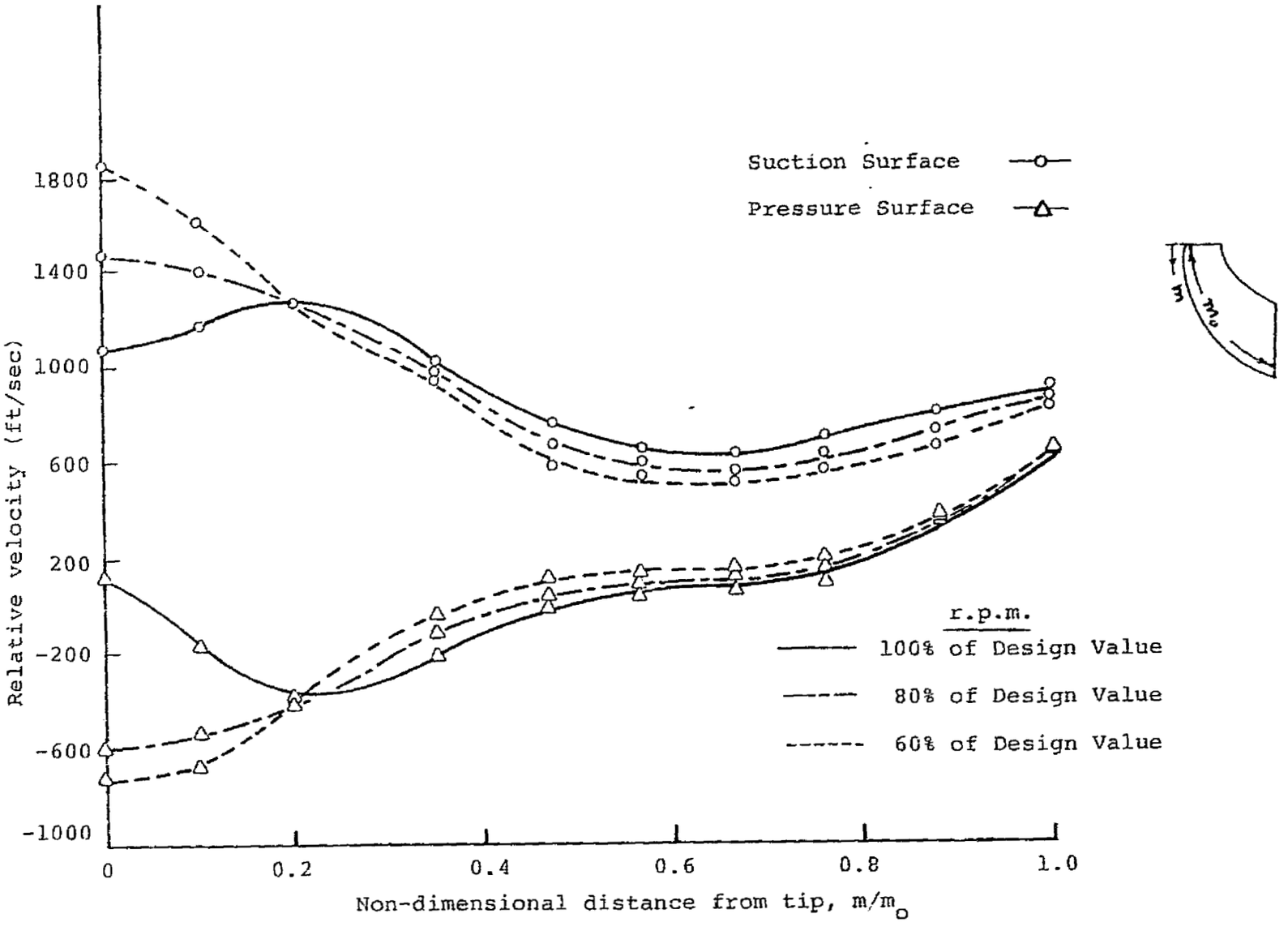

FIGURE 11. VELOCITY DISTRIBUTION NEAR HUB.

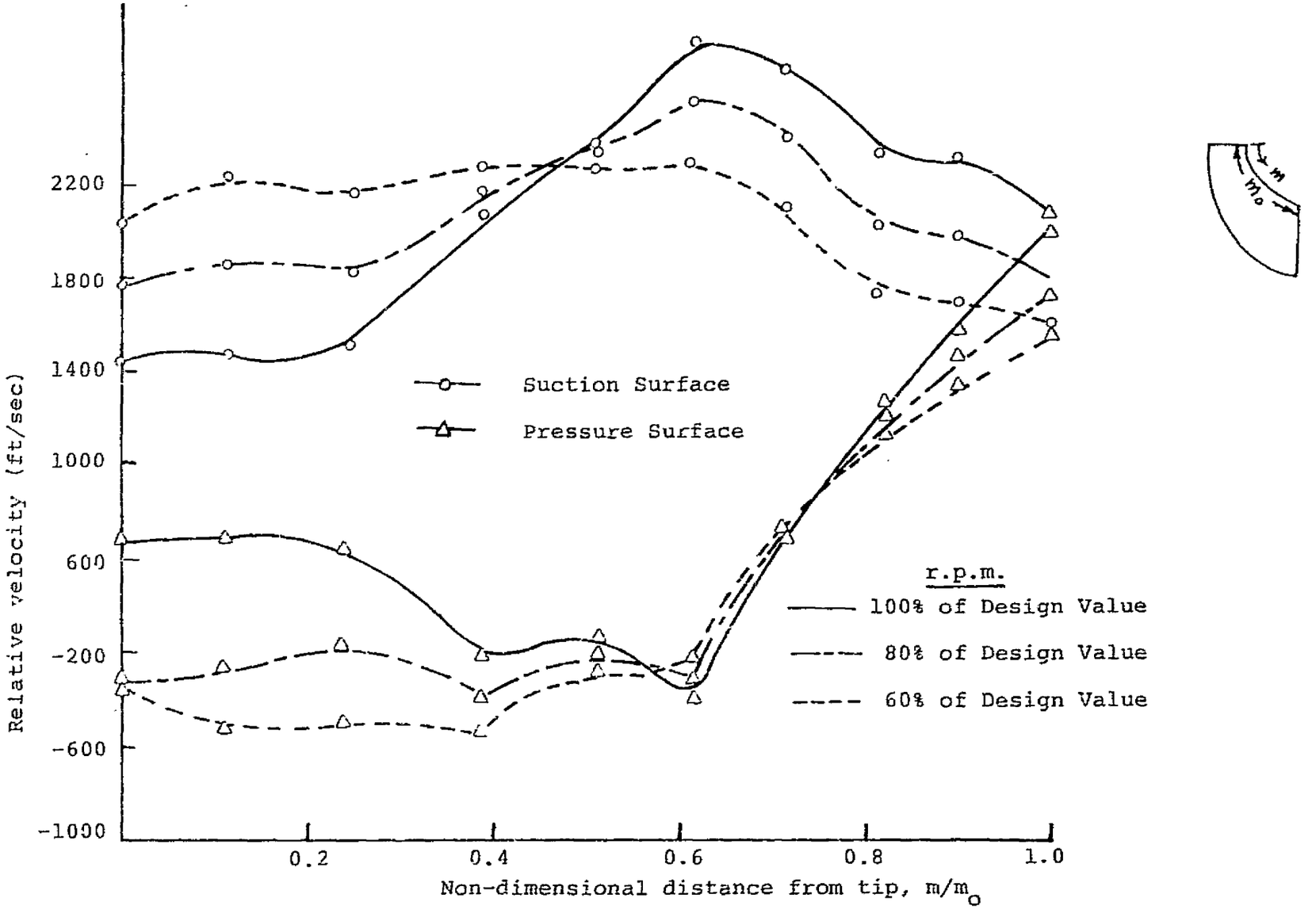

FIGURE 12. VELOCITY DISTRIBUTION NEAR SHROUD.

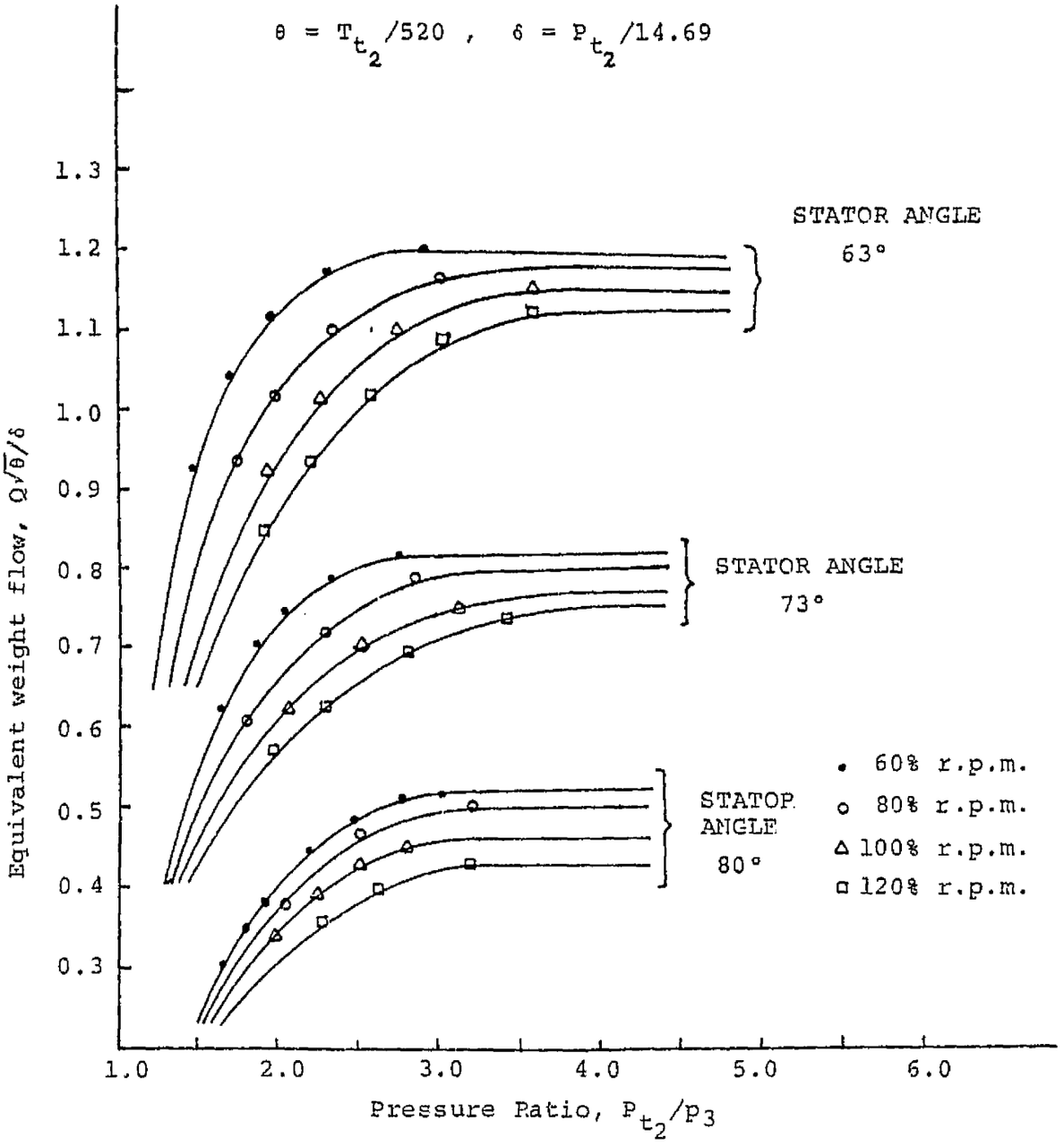

FIG. 13. EFFECT OF VARIABLE STATOR ANGLE ON TURBINE PERFORMANCE.

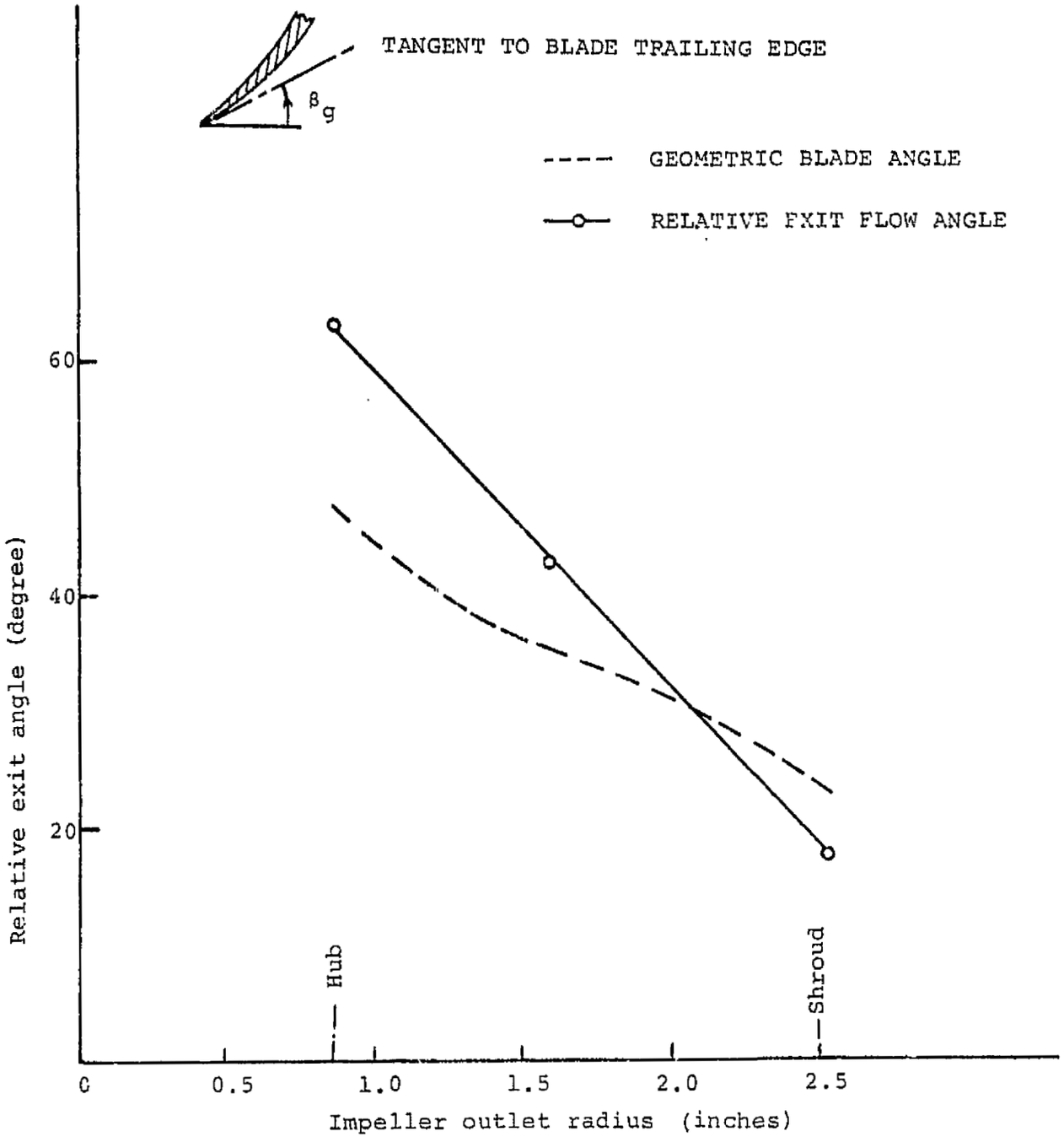

FIGURE 14. RELATIVE EXIT FLOW ANGLE (β_3) AND GEOMETRICAL EXIT ANGLE (β_g), (TAKEN FROM REF. 7).

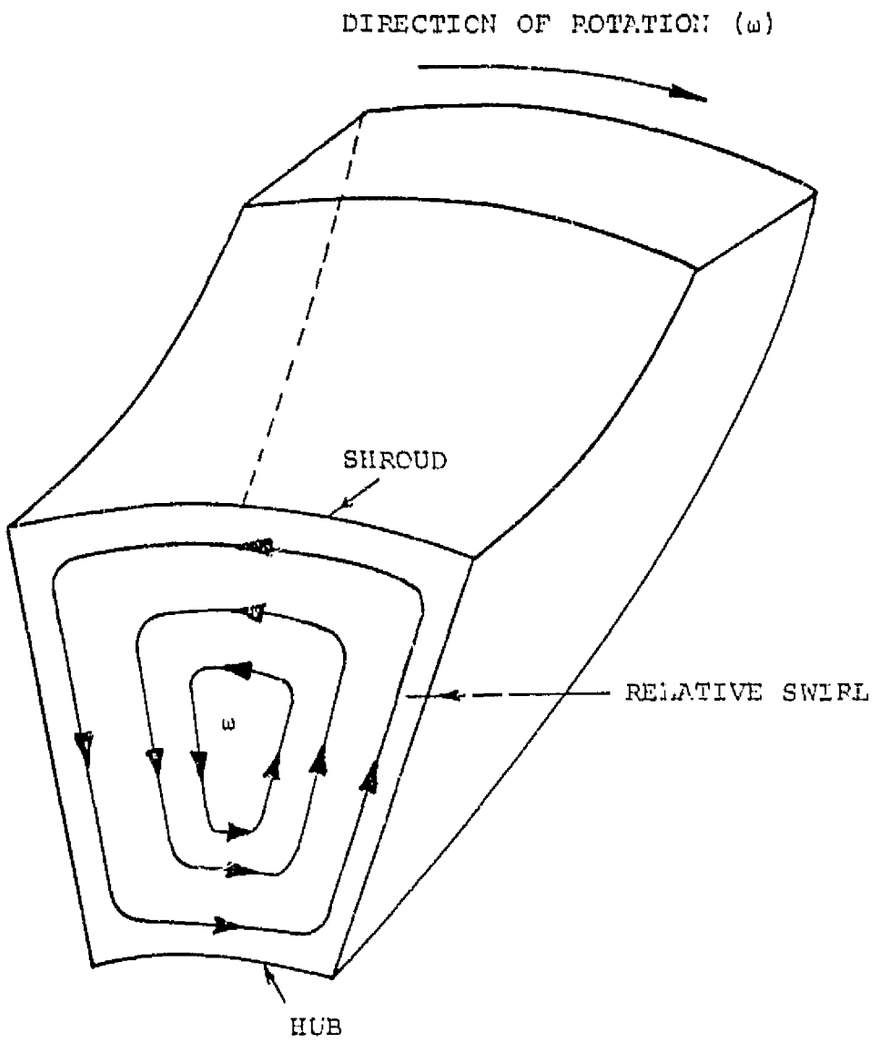

FIG. 15A. ILLUSTRATION OF RELATIVE SWIRL MOTION.

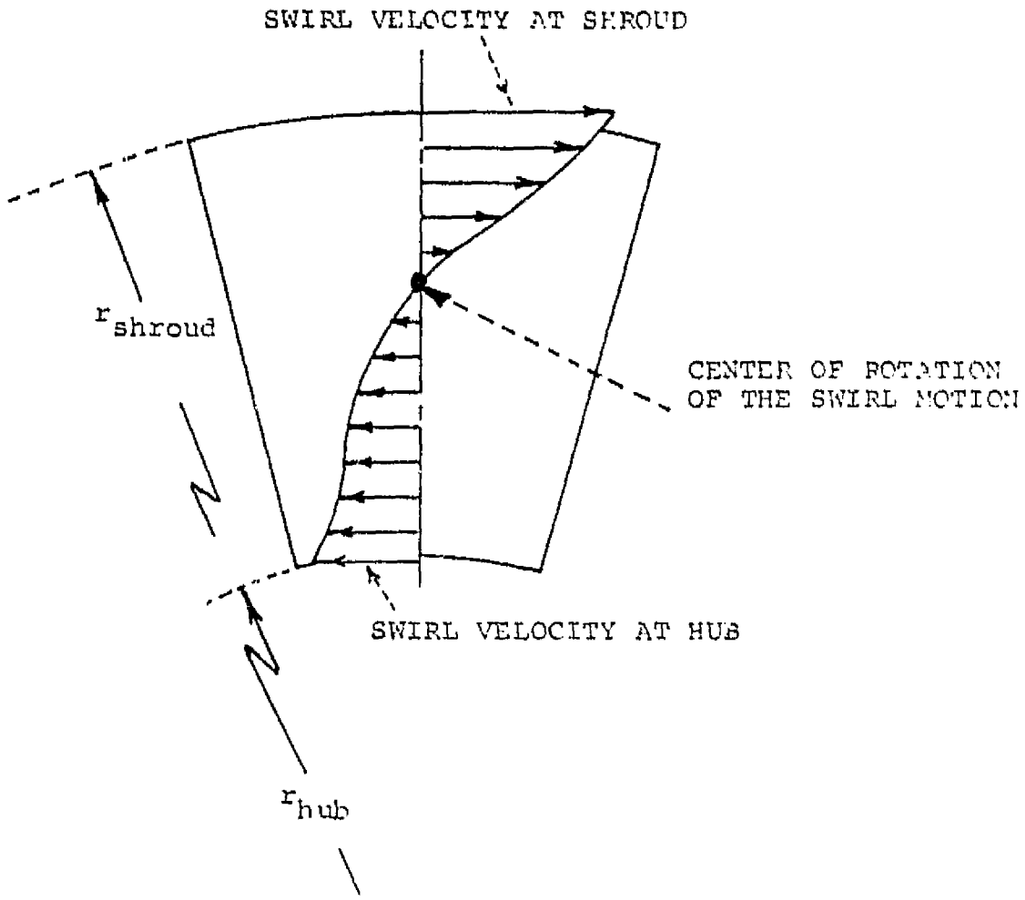

FIG. 15B. TYPICAL DISTRIBUTION FOR THE TANGENTIAL COMPONENT OF RELATIVE SWIRL VELOCITY AT ROTOR EXIT.

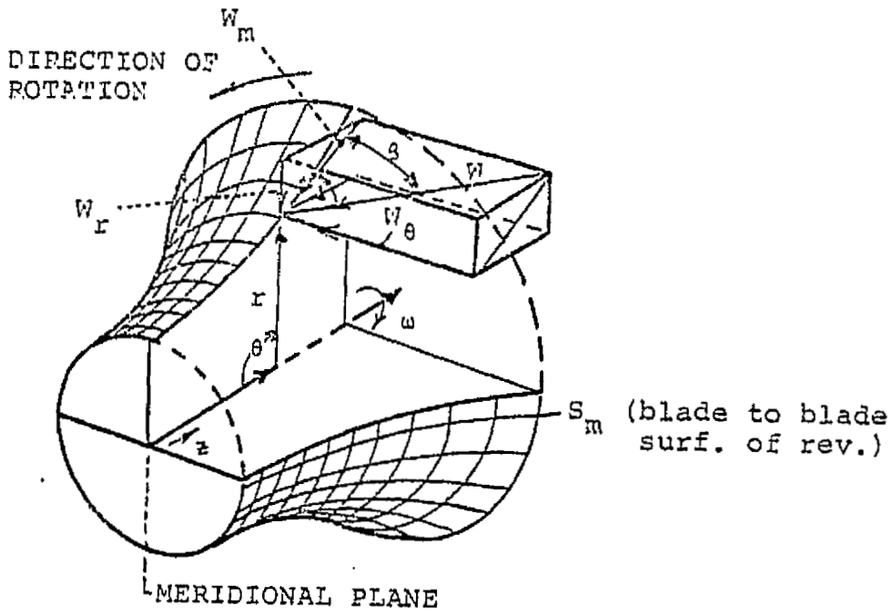

FIGURE 16A. NOMENCLATURE OF RELATIVE FLOW IN RADIAL TURBINE.

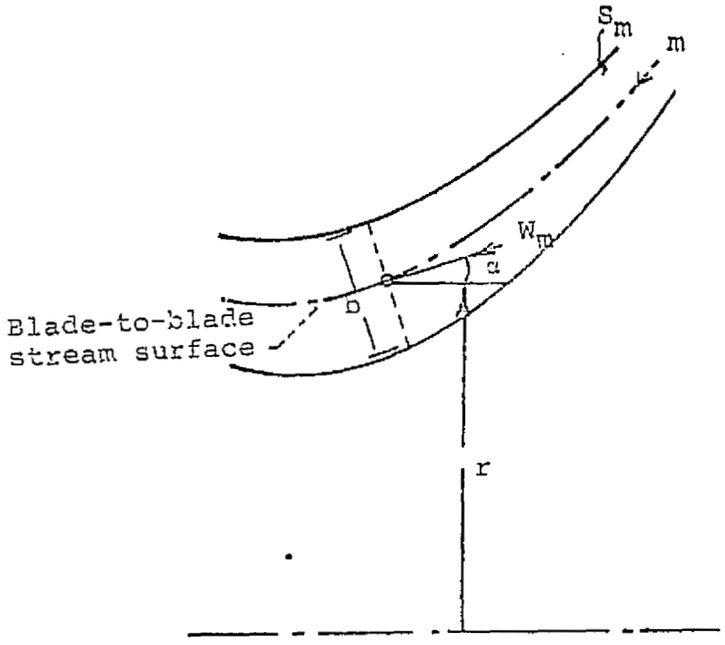

FIGURE 16B. FLOW IN THE FLOW STREAM CHANNEL.

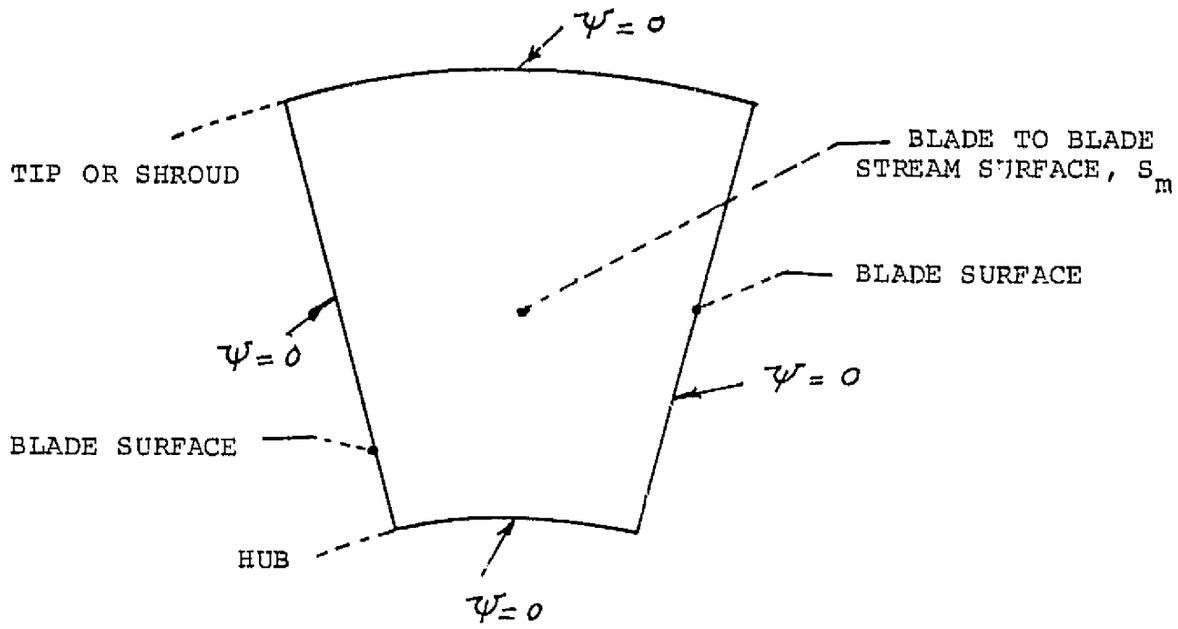

FIG. 16C: BOUNDARY CONDITIONS FOR THE DISPLACEMENT FLOW (RADIAL TURBINE CASE).

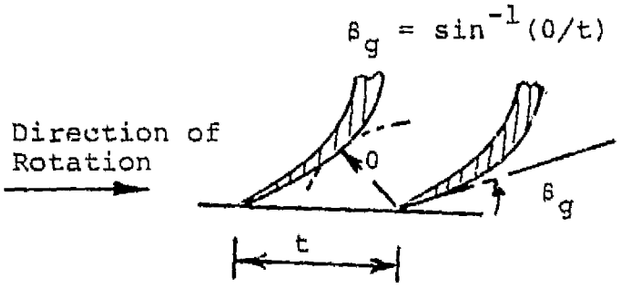

FIGURE 17A. GEOMETRIC BLADE EXIT ANGLE.

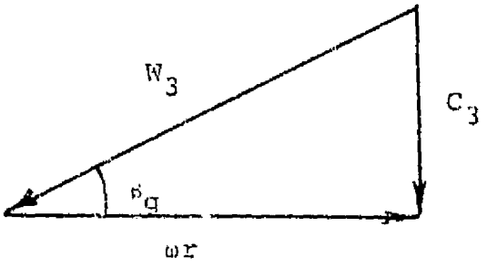

FIGURE 17B. TYPICAL VELOCITY DIAGRAM AT BLADE EXIT (DESIGN POINT).

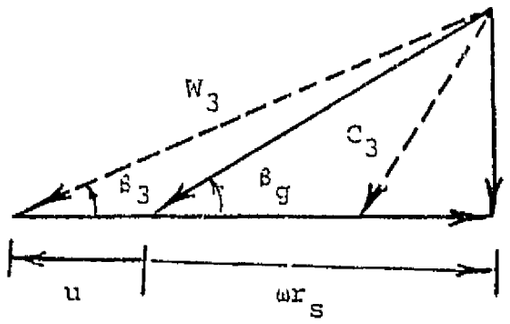

FIGURE 18A. EFFECT OF SWIRL VELOCITY NEAR SHROUD.

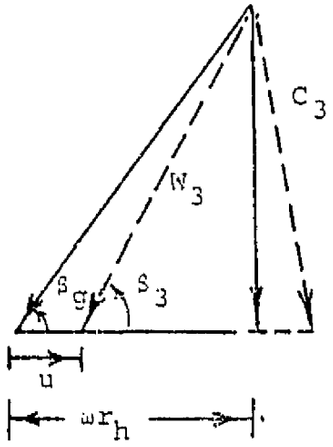

FIGURE 18B. EFFECT OF SWIRL VELOCITY NEAR HUB.

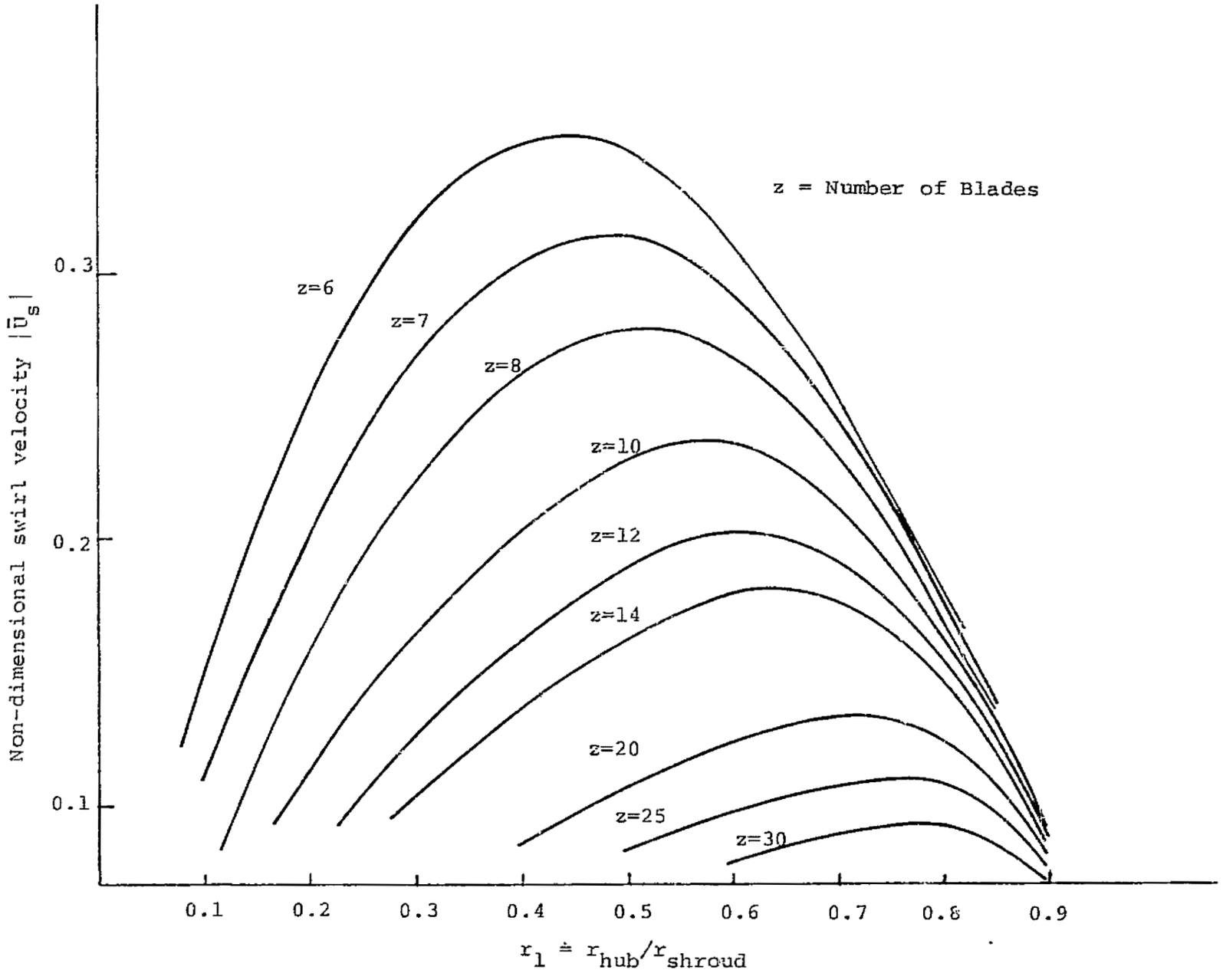

FIG. 19. EFFECT OF DESIGN VARIABLES UPON SWIRL VELOCITY NEAR HUB.

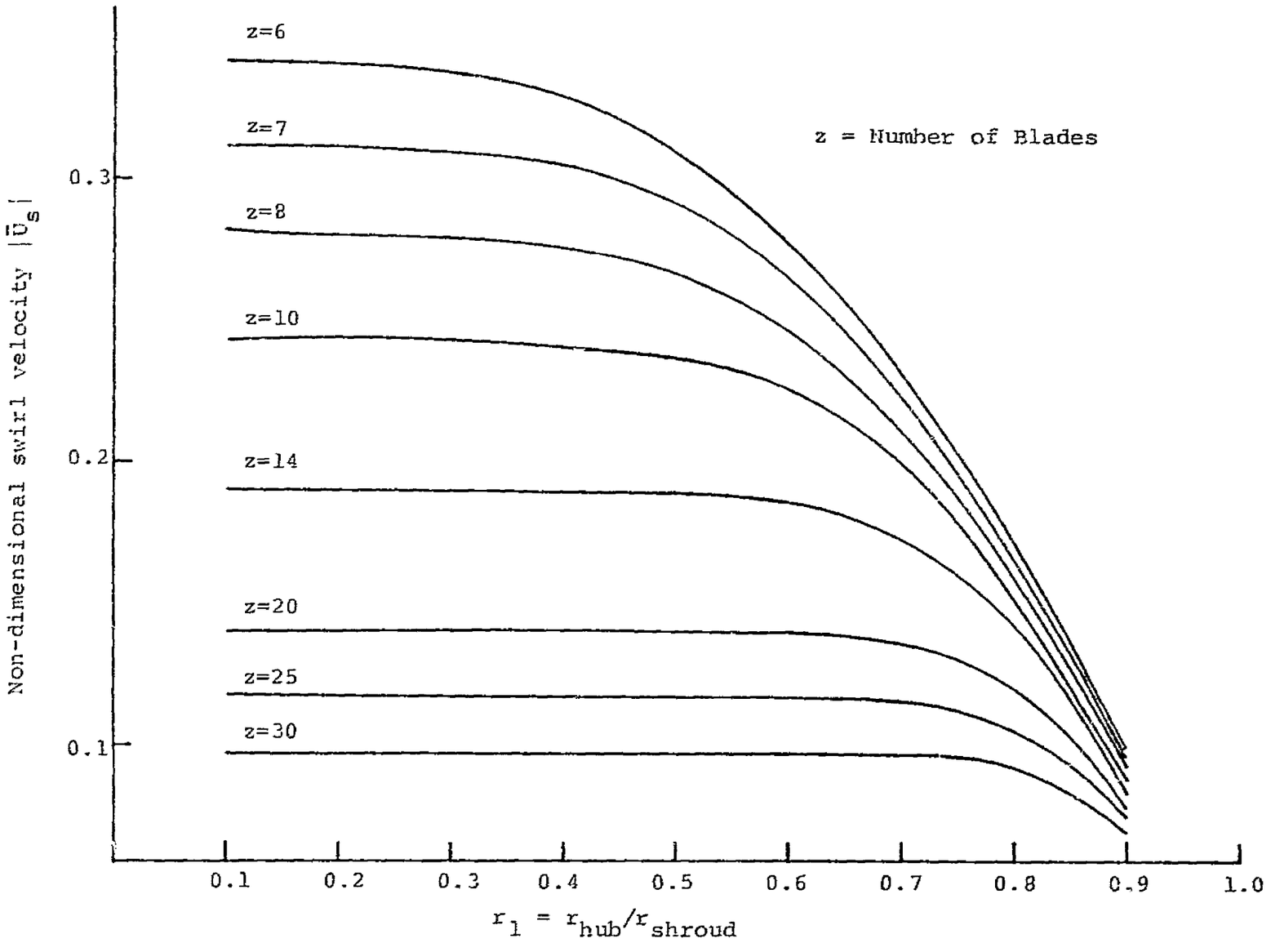

FIG. 20. EFFECT OF DESIGN VARIABLES UPON SWIRL VELOCITY NEAR SHROUD.

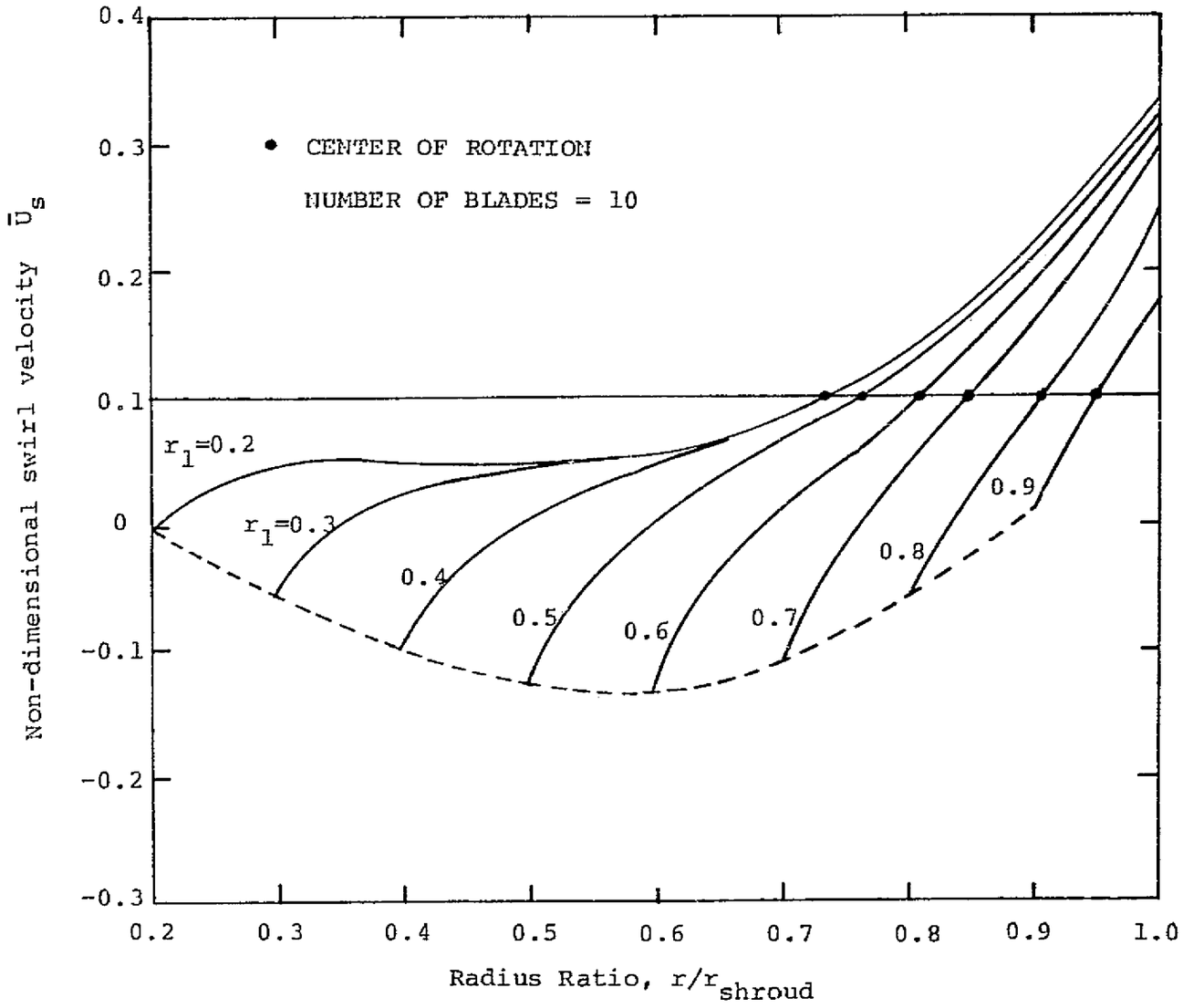

FIG. 21. EFFECT OF CHANGING THE RADIUS RATIO, (r_1)

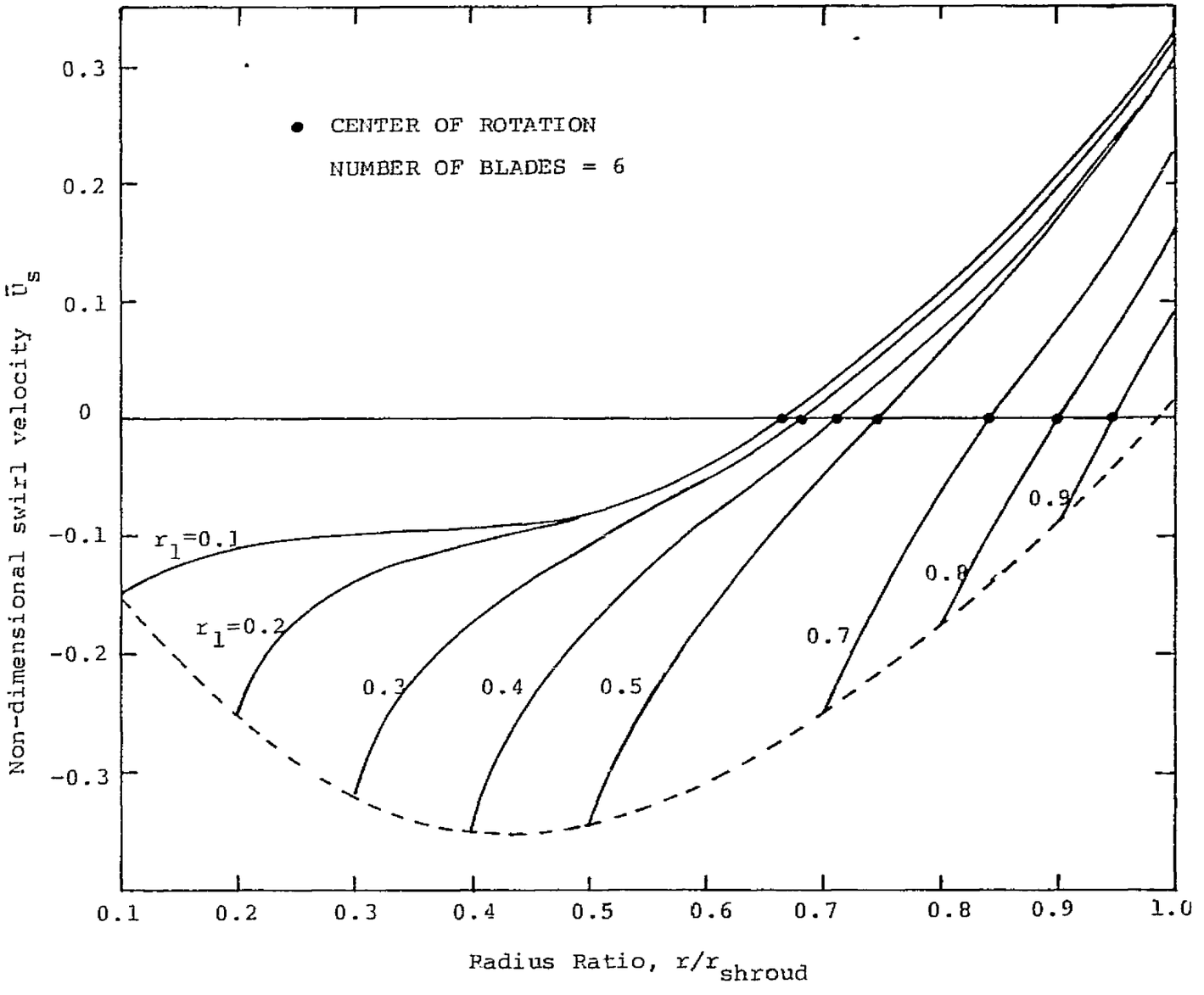

FIG. 22. EFFECT OF CHANGING THE RADIUS RATIO, (r_1)

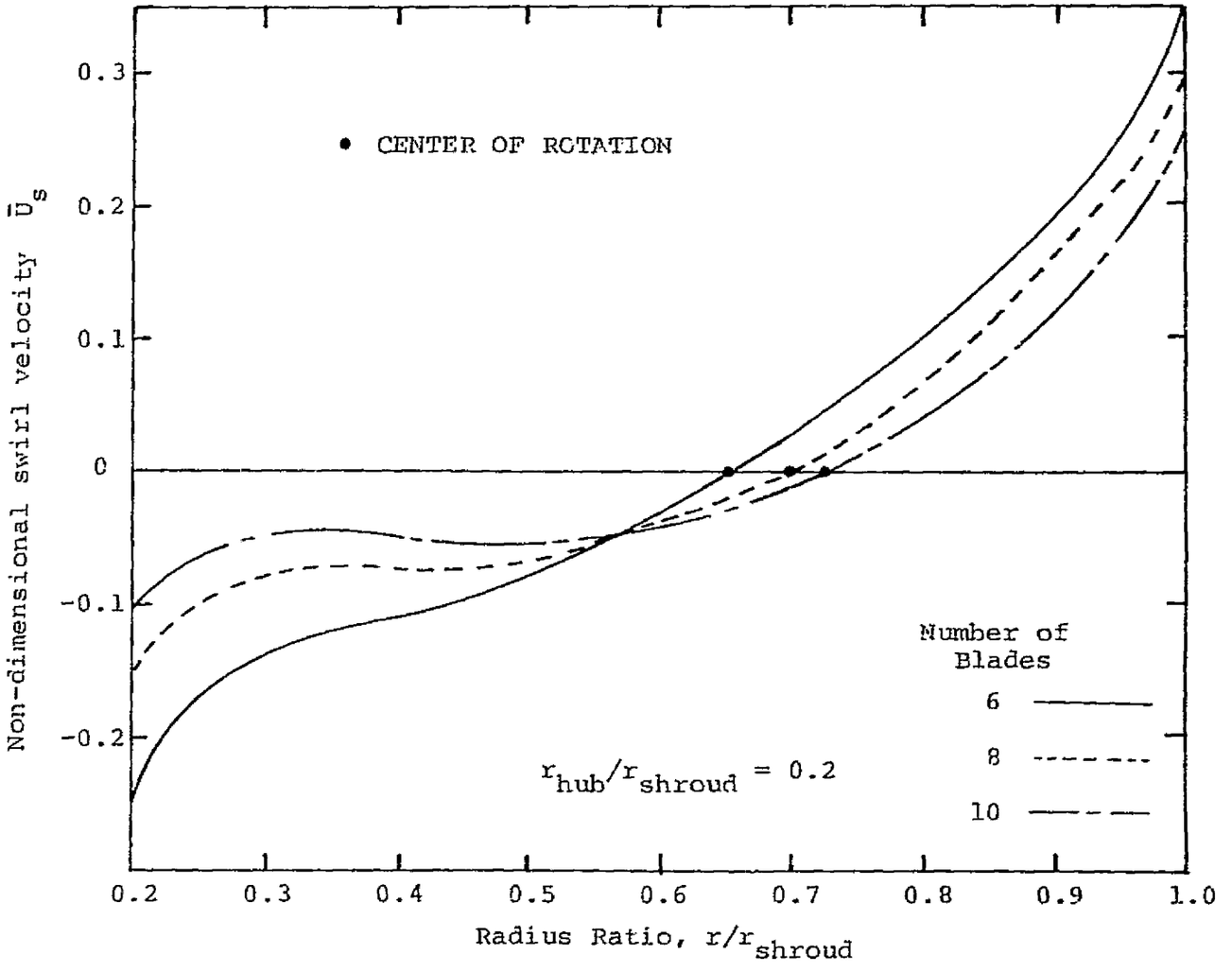

FIG. 23. EFFECT OF CHANGING NUMBER OF BLADES.

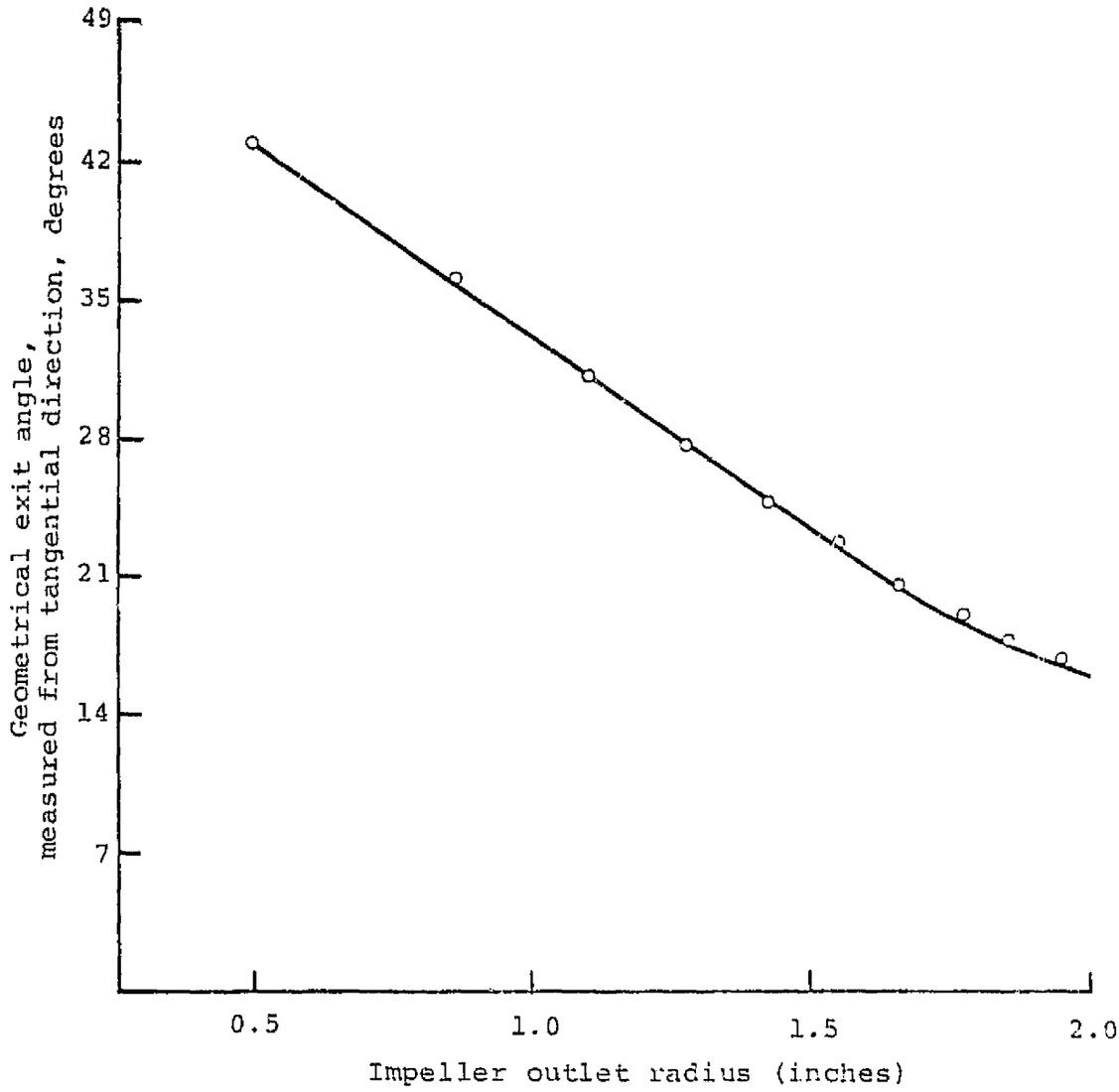

FIG. 24. GEOMETRICAL ANGLE DISTRIBUTION AT ROTOR EXIT.

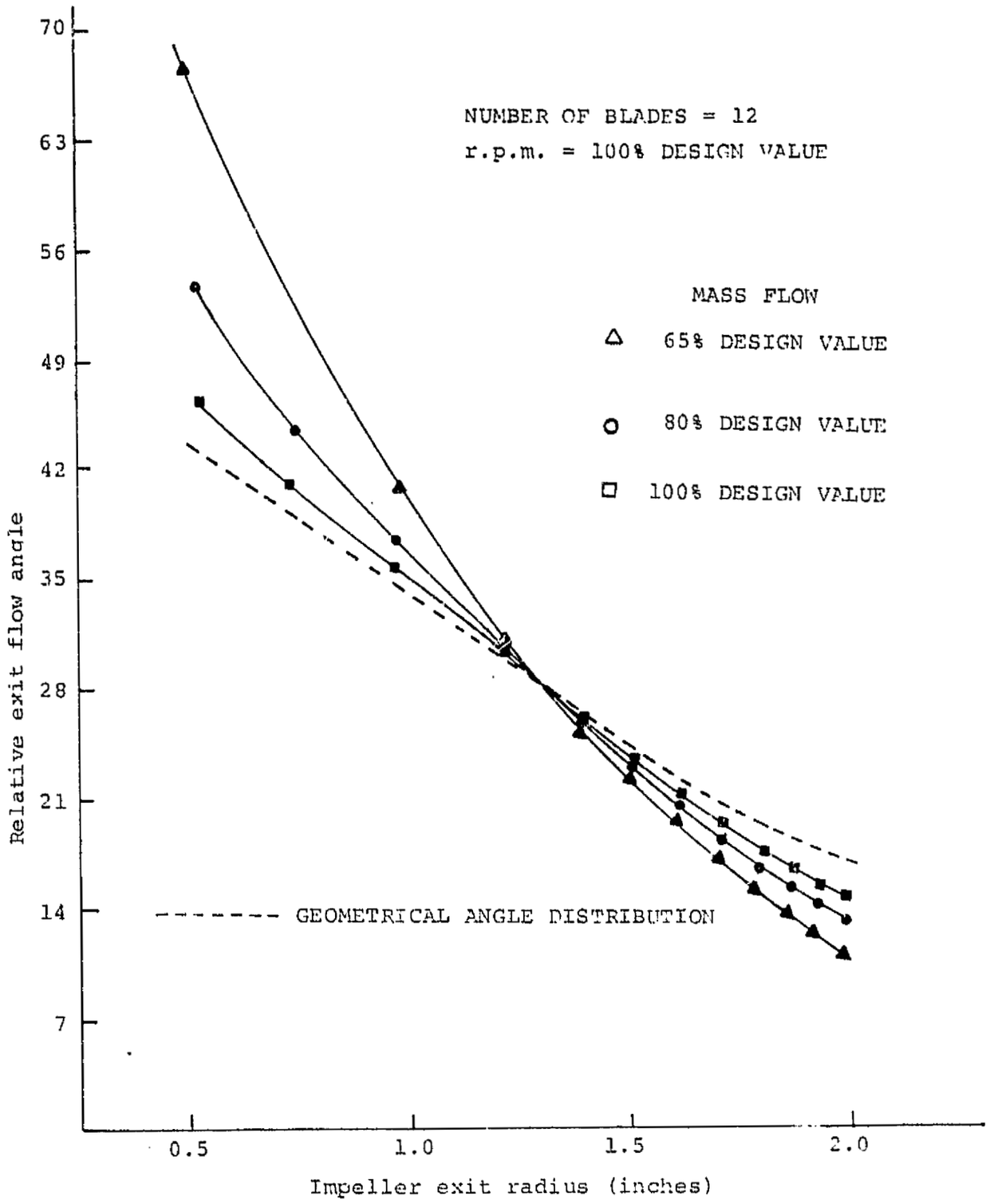

FIG. 25. EFFECT OF CHANGING THE MASS FLOW RATE ON THE EXIT ANGLE DISTRIBUTION.

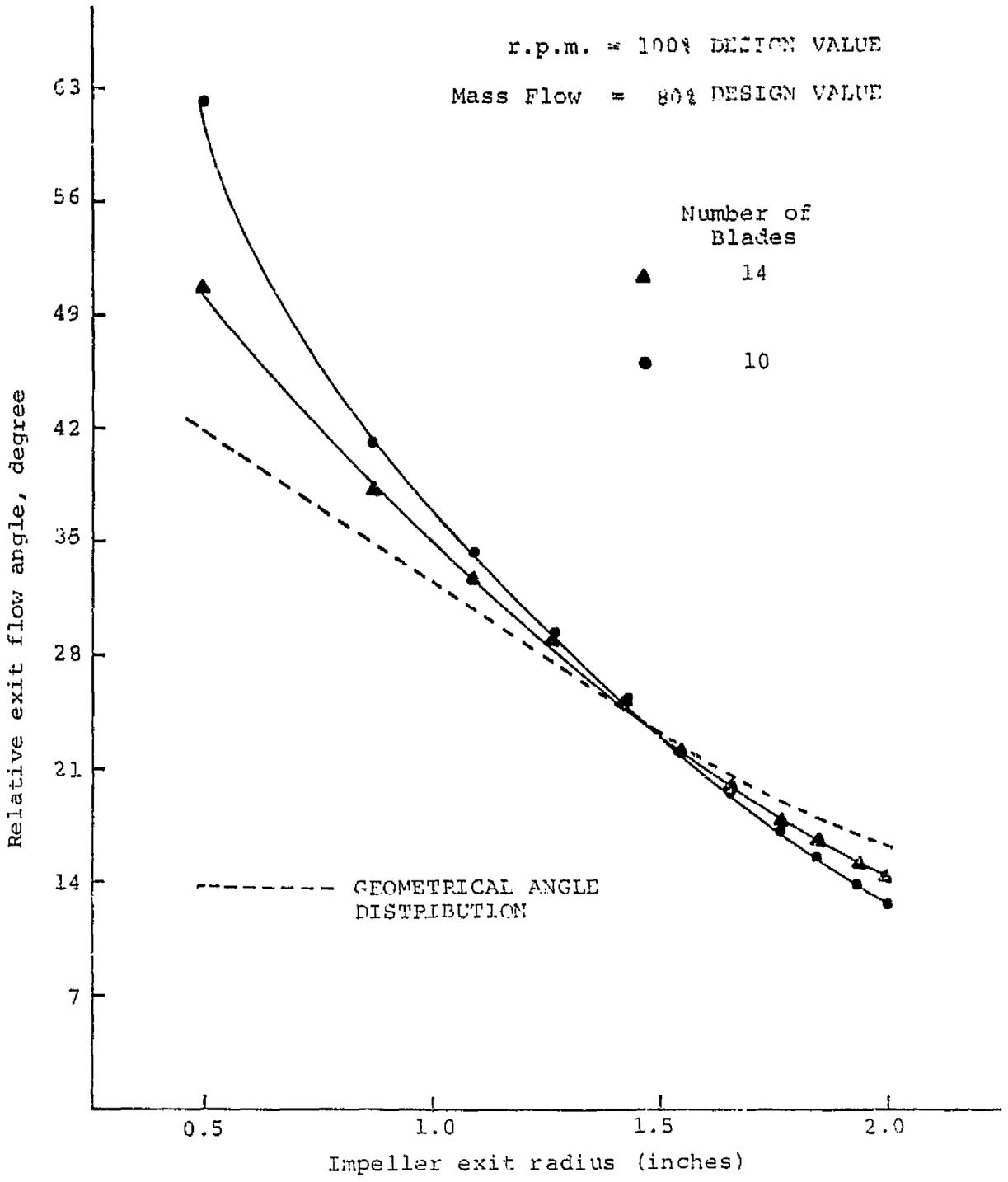

FIG. 26. EFFECT OF NUMBER OF BLADES ON RELATIVE EXIT ANGLE DISTRIBUTION.